

Algorithms for Nonlinear Mixed-Integer Trilateration

Ophir Uziel, Efi Fogel, Dan Halperin, and Sivan Toledo
Blavatnik School of Computer Science and AI, Tel Aviv University

January 1, 2026

Abstract

For three decades, carrier-phase observations have been used to obtain the most accurate location estimates using global navigation satellite systems (GNSS). These estimates are computed by minimizing a nonlinear mixed-integer least-squares problem. Existing algorithms linearize the problem, orthogonally project it to eliminate real variables, and then solve the integer least-square problem. There is now considerable interest in developing similar localization techniques for terrestrial and indoor settings. We show that algorithms that linearize first fail in these settings and we propose several algorithms for computing the estimates. Some of our algorithms are elimination algorithms that start by eliminating the non-linear terms in the constraints; others construct a geometric arrangement that allows us to efficiently enumerate integer solutions (in polynomial time). We focus on simplified localization problems in which the measurements are range (distance) measurements and carrier phase range measurements, with no nuisance parameters. The simplified problem allows us to focus on the core question of untangling the nonlinearity and the integer nature of some parameters. We show using simulations that the new algorithms are effective at close ranges at which the linearize-first approach fails.

Keywords: Integer Ambiguity Resolution, Least-squares Ambiguity Decorrelation Adjustment (LAMBDA), Non-linear, GNSS

1 Introduction

For three decades, carrier-phase observations have been used to obtain the most accurate location estimates using global navigation satellite systems (GNSS) (Teunissen 1995; Teunissen 2017; Xu, Cannon, and Lachapelle 1995; Chang and Paige 2003). While originally designed for measuring the signal’s time of arrival (ToA), which varies linearly with the range (distance) between the emitting satellite and the receiver, it turns out that the receiver can also measure and track the carrier’s phase, which also varies linearly with the range, but wraps around every whole wavelength. The errors in the phase measurements are orders of magnitude smaller than in the ToA estimates, when both are expressed in meters, allowing in principle more accurate location estimates. However, to resolve the location of the receiver from carrier-phase measurements, the receiver needs to resolve the so-called *integer ambiguities*, essentially the number of whole wavelengths between each satellite and the receiver (the actual formulation also involves nuisance parameters, such as the initial phases at the satellite and the receiver). A method called LAMBDA (Teunissen 1995; De Jonge and Tiberius 1996) was invented to efficiently resolve the integer ambiguities. There are also some variants that have been shown to be effective (Xu, Cannon, and Lachapelle 1995; Borno, Chang, and Xie 2014; Chang and Paige 2003; Chang, Yang, and Zhou 2005; Xie, Chang, and Al Borno 2012). These methods work well in both single-epoch settings and in multi-epoch settings in which the receiver is either stationary or moving (in the latter setting the method is referred to as real-time kinematic positioning, or RTK).

There is now considerable interest in developing carrier-phase positioning for terrestrial localization systems, where the distances between the emitters and the receivers are much smaller than in GNSS, including in cellular and indoor systems (Wymeersch, Amiri, and Seco-Granados 2023; Fan et al. 2022; Nikonowicz et al. 2024). Recent articles on short-range carrier localization that discuss the integer-ambiguities resolution problem propose using LAMBDA and its variants, implicitly assuming that these methods are suitable for this setting (Zhang, Kang, and Zhang 2021; Wymeersch, Amiri, and Seco-Granados 2023; Fan et al. 2022).

We show in this paper that this assumption is often wrong. LAMBDA and its variants start by linearizing a nonlinear mixed-integer least-squares problem around an approximate solution of the continuous (non-integer) constraints. The nonlinearity is the Euclidean distance between the emitter and receiver, which is very large in GNSS. Therefore, in GNSS settings the linearization introduces essentially no error, even if the approximate solution (usually obtained from ToA measurements) is not very accurate. In terrestrial and indoor settings, where

the distances between the emitters and receivers are on the order of meters or kilometers, this is no longer true; we show below that LAMBDA variants fail at these distances.

In some cases the linearization is not explicit. Constraints that relate the unknown parameters to observations and to an approximate solution can also be derived from geometric principles (see, e.g. (Chang and Paige 2003)). However, these constraints are also approximations that assume that the distances to the satellites is very large. In general, both approaches lead to the same constraints.

The main contributions of this paper are two families of algorithms for resolving the integer ambiguities in trilateration problems that include both range measurements and carrier-phase range measurements. Our algorithms tackle the nonlinearity head-on. One family of algorithms is based on elimination of the nonlinear terms. We use a non-linear elimination technique, reminiscent of closed-form solutions for code-phase GNSS localization (Bancroft 1985; Sirola 2010). The elimination process reduces the original problem to a linear least-squares problem with discrete parameters that are not integers. We show that a key component of LAMBDA, namely the Schnorr-Euchner search (Schnorr and Euchner 1994), can be adapted to this case. This generalization of the Schnorr-Euchner search is another key contribution of this article. When the target is tracked over two or more epochs, the non-linear elimination includes two subtraction (differencing) stages. This leads to a generalized mixed-integer least-squares minimization problem; the discrete parameters are integers, as in LAMBDA.

A second family of algorithms, described in Section 7, uses geometric arrangements to resolve the ambiguities. These algorithms essentially project the integers onto the 2D or 3D space of target locations. Interestingly, these algorithms run in polynomial time even in the worst case, even though LAMBDA reduces the mixed-integer localization problem to a pure integer least-square problem which is known to be NP hard (Agrell et al. 2002; Micciancio 2001; Emde Boas 1981) and hard to approximate (Dinur et al. 2003). The reason for this surprising result is the projection to 2D or 3D, which allows us to enumerate all the combinations of integers that correspond to actual locations of the target in polynomial time. This is another important contribution of this article.

We show in simulations that our methods are both efficient and effective, and that they can resolve the integer ambiguities at ranges where LAMBDA fails due to the linearization error.

We focus on trilateration problems that include range observations and observations of the remainders of division of the ranges by the wavelength. These problems are simpler than GNSS localization problems in that they lack nuisance parameters such as clock bias and initial phases at the emitters and receiver. (The lack of these nuisance parameters also means that measurements at a reference receiver whose location is known are not necessary.)

We chose to focus on these simplified localization problems, which still retain the Euclidean nonlinearity and the mixture of real and integer parameters, to enable the widest possible exploration of the algorithmic design space. We plan to explore localization problems associated with realistic system models and to extend our algorithms to these cases in the near future.

In summary, the main contributions of this article are:

1. A square-and-difference elimination algorithm that transforms the mixed-integer trilateration problems defined in Section 2 to linear least-squares problems with discrete (but not integer) parameters.
2. An extension of the Schnorr-Euchner search that can solve discrete linear least-squares problems of this type exactly, possibly in exponential time (just like the original Schnorr-Euchner search for integer least-squares problems).
3. A square and double-difference elimination algorithm that transforms multi-epoch problems, also defined in Section 2, into linear mixed-integer least-squares problems, which can be solved using LAMBDA and its variants.
4. Careful characterization of the uncertainties and errors introduced in the elimination processes, which allows us to correctly weigh the constraints in the linear least-square problems. These weights are critical for the success of the algorithms.
5. Several geometric algorithms for solving the same trilateration problems. These algorithms project the problems, including the integer parameters, into 2 or 3 dimensions. These algorithms run in polynomial time, even though LAMBDA and its variants, as well as the algorithms from items 1 and 3 in this list, reduce the localization problem into an NP-hard integer least-squares problem.
6. Computational demonstration, using simulations, that our algorithms are efficient and effective.

The rest of this article is organized as follows. Section 2 defines the estimation problems that we tackle and the concrete values or ranges of parameters under which we test our algorithms. Sections 3, 4, 5, and 6 together

present our square-and-difference algorithms. More specifically, Section 3 explains how we derive constraints from the raw observations. This section describes all the elimination techniques that we use. Section 4 specifies how we assemble these constraints, which are all equality constraints with error or noise terms, into generalized least-squares minimization problems. Section 5 characterizes each of the error terms; these characterizations determine the weight of each constraint in the minimization problems. Section 6 presents the generalized Schnorr-Euchner search, which we use to solve mixed-discrete least squares problems. Section 7 presents our polynomial-time geometric algorithms. Section 8 describe the performance of both our new algorithm and LAMBDA on simulated data. Section 9 presents our conclusions from this research.

2 Problem Statement

We wish to localize a target at Cartesian coordinates $\hat{\ell} = [x \ y \ z]^T$ or $\hat{\ell} = [x \ y]^T$ from range or pseudo-range measurements from a set of reference points $\rho_i = [x_i \ y_i \ z_i]^T$ or $\rho_i = [x_i \ y_i]^T$, as well as carrier-phase measurements from the same reference points. The ring above the letter ℓ marks this location as the ground truth. The simplest setting for such problems consists of a set of range and carrier-phase observations

$$r_i = \left\| \hat{\ell} - \rho_i \right\|_2 + \epsilon_i \quad (1)$$

$$\lambda\varphi_i + \lambda\hat{n}_i = \left\| \hat{\ell} - \rho_i \right\|_2 + \delta_i, \quad (2)$$

where r_i is a noisy range (distance) measurement, ϵ_i is the range-measurement error (noise), λ is the wavelength of the carrier wave of the signal emitted by the references (or by the target, in transmitter localization), $\varphi_i \in [0, 1)$ is a noisy phase measurement, δ_i is the phase measurement error and $\hat{n}_i \in \mathbb{N}$ is an unknown integer that corresponds roughly to the number of whole wavelengths between $\hat{\ell}$ and ρ_i . (Because of the measurement error, $\hat{n}_i = \lfloor (\|\hat{\ell} - \rho_i\| - \delta_i)/\lambda \rfloor$ can be smaller or larger by one than $\lfloor \|\hat{\ell} - \rho_i\|/\lambda \rfloor$.) The unknown integer parameters are often called *integer ambiguities*. In more realistic problems only pseudo-ranges are measured $\|\hat{\ell} - \rho_i\| + c\Delta t$ where Δt is a clock error or bias and c is the speed of propagation) and the phases are measured relative to some unknown initial phases at both the transmitter and the receiver. There might also be complications from ionospheric delays, tropospheric delays, etc.

If the receiver makes observations of the forms (1) and (2) at multiple points in time, called *epochs*, and can track the carrier phases continuously, we denote the observations at time j

$$r_{i,j} = \left\| \hat{\ell}_j - \rho_{i,j} \right\|_2 + \epsilon_{i,j} \quad (3)$$

$$\lambda\varphi_{i,j} + \lambda\hat{n}_i = \left\| \hat{\ell}_j - \rho_{i,j} \right\|_2 + \delta_{i,j}. \quad (4)$$

Note that this notation allows both the target and the references to change their locations between epochs, but that a single integer is used in all the phase observations of reference i . In some settings we know that the target and/or the references are stationary; it is easy to exploit this information, as we shall see below.

The assumption that a but that a single integer \hat{n}_i is used in all the phase observations of reference i depends on the receiver's ability to track the carrier phase continuously; that is, that there are no *cycle slips* (the term used in the GNSS literature to describe a failure to track the carrier phase continuously).

These problems are interesting when $\delta_i \ll \epsilon_i$. Typical value of λ for radio systems range from about 1 m to about 10 cm and typical standard deviations for δ_i are on the scale of $\lambda/100$, so about 1 cm to 1 mm. In GNSS typical standard deviations for ϵ_i are on the scale of 10 m, much higher.

We wish to estimate $\hat{\ell}$ in the generalized least-squares sense, which corresponds to maximum likelihood under the assumptions that the ϵ_i s and δ_i s are unbiased Gaussian random variables. We further assume that the ϵ_i s and δ_i s are uncorrelated and have known standard deviations $\sigma(\epsilon_i)$ and $\sigma(\delta_i)$. Under these assumptions, we seek the minimizer

$$\hat{\ell}, \hat{n} = \arg \min_{\ell, n} \left\| W \left(M(\ell) - \begin{bmatrix} 0 \\ \lambda I \end{bmatrix} n - \begin{bmatrix} r \\ \lambda\varphi \end{bmatrix} \right) \right\|_2 \quad (5)$$

where W is a diagonal matrix with $\sigma^{-1}(\epsilon_i)$ and $\sigma^{-1}(\delta_i)$ on the diagonal, and M is a function such that

$$M_i(\ell) = M_{m+i}(\ell) = \|\ell - \rho_i\|_2,$$

where m is the number of references. Note that we use the plain letters ℓ and n to denote hypothetical locations and integer vectors, and that we decorate ℓ and n with a hat to denote the estimates. The integer vector \hat{n} is a vector of nuisance parameters; we normally do not need to estimate it, but algorithms for estimating $\hat{\ell}$ usually estimate \hat{n} it as a side effect.

We can obtain a coarse estimate ℓ_0 of $\hat{\ell}$ from the range measurements alone and linearize M around ℓ_0 ,

$$M(\ell) \approx M(\ell_0) + J_M(\ell - \ell_0) = M(\ell_0) + \frac{\partial M}{\partial \ell}(\ell - \ell_0)$$

where $J_M = \partial M / \partial \ell$ is the Jacobian of M and where the derivatives are evaluated at ℓ_0 . In GNSS, the distances $\|\hat{\ell} - \rho_i\|$ are 20,000 km or more, so when ℓ_0 is within tens or even hundreds of meters of ℓ , this linear approximation is superb (see Section 5.4 below), so we can estimate $\hat{\ell}$ and \hat{n} by solving the mixed-integer linear least-squares problem

$$\arg \min_{\Delta \ell, n} \left\| W \left(M(\ell_0) + J_M \Delta \ell - \begin{bmatrix} 0 \\ \lambda I \end{bmatrix} n - \begin{bmatrix} r \\ \lambda \varphi \end{bmatrix} \right) \right\|_2, \quad (6)$$

where $\Delta \ell = \ell - \ell_0$. Note that the same W appears in this expression, because the linearization errors at GNSS ranges are so small that their effect on the overall errors is negligible.

We are interested in problems in which the ranges are much smaller, where the linear approximation may not be good enough. In other words, in GNSS a reasonably good ℓ_0 allows us to ignore the nonlinearity in M . The main and essentially only computational challenge is the estimation of the integer ambiguities \hat{n} . This is true even if there are additional nuisance parameters like clock bias, because the dependence on them is linear.

We note that in multi-epoch problems, ℓ_0 can also be estimated from both range measurements and carrier-phase measurements, ignoring the fact that the elements of n are integers. When the number of references and/or epochs is large, this approach can sometimes generate a more accurate ℓ_0 than using the range measurements alone, and hence can allow the linearization-first approach to work at shorter ranges (Chang and Paige 2003). We focus in this paper on single-epoch and two-epoch problems, in which technique is rarely effective, and on problems in which the nonlinearity must be tackled head on.

2.1 Parameters for Experimental Evaluations

We use parameter values that are typical in GNSS, except for the distances to the references. More specifically, our baseline values are

$$\begin{aligned} \lambda &= 19 \text{ cm} \\ \sigma(\epsilon_i) &= 10 \text{ m} \\ \sigma(\delta_i) &= 0.1^\circ = 19/3600 \text{ cm} \\ \sigma \left| \hat{\ell} - \ell_0 \right|_j &= 10 \text{ m} \\ \left\| \hat{\ell} - \rho_i \right\| &\approx 10 \text{ m to } 20,000 \text{ km} \end{aligned}$$

We test the algorithms in 2D and in 3D. In our simulations, we select $\hat{\ell} - \ell_0$ at random from a Gaussian distribution of each coordinate. We select the ρ_i s by selecting a uniform random azimuth from ℓ , selecting a point on a circular orbit at that azimuth, and then perturbing the coordinates by adding random Gaussian noise to each coordinate of ρ_i . The standard deviation of these perturbations is 10% of the nominal range.

3 Deriving Linear Constraints

Our observations (1) and (2) are nonlinear in $\hat{\ell}$ and they include both continuous parameters, the coordinates of $\hat{\ell}$, and integer parameters, the \hat{n}_i s. We present in this section several techniques to derive from these observations constraints that are linear in both $\hat{\ell}$ and in a vector of m discrete parameters. In the multi-epoch setting, the discrete parameters are simply the \hat{n}_i s, which are integers, but in the single-epoch setting they are not integers.

Our derived constraints are all mathematical equalities with error terms. The error terms are denoted clearly and we quantify them in Section 5 below. Error terms that are functions of δ_i are denoted $\delta_i^{(\dots)}$, where letters within the parentheses specify the error expression, error terms that are functions of ϵ_i are denoted $\epsilon_i^{(\dots)}$, and error terms that depend on neither δ_i nor ϵ_i are denoted η_i or $\eta_i^{(\dots)}$.

3.1 Squared Phase Observations

Squaring Equation (2)

$$\lambda(\hat{n}_i + \varphi_i) = \left\| \hat{\ell} - \rho_i \right\|_2 + \delta_i.$$

we obtain

$$\lambda^2(\hat{n}_i + \varphi_i)^2 = \left\| \hat{\ell} - \rho_i \right\|_2^2 + 2\delta_i \left\| \hat{\ell} - \rho_i \right\|_2 + \delta_i^2. \quad (7)$$

We treat $2\delta_i \left\| \hat{\ell} - \rho_i \right\|_2$ as an error term denoted $\delta_i^{(s)}$, the letter 's' denoting the squaring operation. We use this constraint as is in multi-epoch problems, as a building block for further transformations:

$$\lambda^2(\hat{n}_i + \varphi_i)^2 = \left\| \hat{\ell} - \rho_i \right\|_2^2 + \delta_i^{(s)} + \delta_i^2. \quad (8)$$

In single-epoch settings, we change the discrete variables. We substitute $\hat{s}_i = (\hat{n}_i + \varphi_i)^2$ to obtain

$$\lambda^2 \hat{s}_i = \left\| \hat{\ell} - \rho_i \right\|_2^2 + \delta_i^{(s)} + \delta_i^2. \quad (9)$$

3.2 Squared Range Observations

We can also square the range observations (2)

$$r_i = \left\| \hat{\ell} - \rho_i \right\|_2 + \epsilon_i$$

to obtain

$$\begin{aligned} r_i^2 &= \left\| \hat{\ell} - \rho_i \right\|_2^2 + 2\epsilon_i \left\| \hat{\ell} - \rho_i \right\|_2 + \epsilon_i^2 \\ &= \left\| \hat{\ell} - \rho_i \right\|_2^2 + \epsilon_i^{(s)} + \epsilon_i^2, \end{aligned} \quad (10)$$

where $\epsilon_i^{(s)} = 2\epsilon_i \left\| \hat{\ell} - \rho_i \right\|_2$.

3.3 Differencing Squared Observations by Reference

Subtracting squared observations associated with different references eliminates the nonlinearity in $\hat{\ell}$. Subtracting the squared phase constraint of reference 1 from that of reference i , we obtain

$$\lambda^2 \left((\hat{n}_i + \varphi_i)^2 - (\hat{n}_1 + \varphi_1)^2 \right) = \left\| \hat{\ell} - \rho_i \right\|_2^2 - \left\| \hat{\ell} - \rho_1 \right\|_2^2 + \delta_i^{(s)} + \delta_i^2 - \delta_1^{(s)} - \delta_1^2. \quad (11)$$

Expanding the squared norms on the right-hand side gives

$$\begin{aligned} \left\| \hat{\ell} - \rho_i \right\|_2^2 - \left\| \hat{\ell} - \rho_1 \right\|_2^2 &= (\hat{\ell} - \rho_i)^T (\hat{\ell} - \rho_i) - (\hat{\ell} - \rho_1)^T (\hat{\ell} - \rho_1) \\ &= -2\hat{\ell}^T (\rho_i - \rho_1) + \rho_i^T \rho_i - \rho_1^T \rho_1. \end{aligned} \quad (12)$$

The subtraction eliminated the squares $\hat{\ell}^T \hat{\ell} = x^2 + y^2 + z^2$ (or $\hat{\ell}^T \hat{\ell} = x^2 + y^2$ in 2D), leaving us with a expression that is a linear function of the unknown vector $\hat{\ell}$.

In the single-epoch setting this results in a constraint that is linear in both $\hat{\ell}$ and the discrete-valued parameters \hat{s}_i ,

$$\lambda^2 \hat{s}_i - \lambda^2 \hat{s}_1 = -2\hat{\ell}^T (\rho_i - \rho_1) + \rho_i^T \rho_i - \rho_1^T \rho_1 + \delta_i^{(s)} + \delta_i^2 - \delta_1^{(s)} - \delta_1^2 \quad (13)$$

(the error terms $\delta_i^{(s)}$ and $\delta_1^{(s)}$ also depend on $\hat{\ell}$; we analyze this dependence in Section 5.2 below). In the multi-epoch setting we stay with a constraint that is still nonlinear in the n_i s,

$$\lambda^2 \left((\hat{n}_i + \varphi_i)^2 - (\hat{n}_1 + \varphi_1)^2 \right) = -2\hat{\ell}^T (\rho_i - \rho_1) + \rho_i^T \rho_i - \rho_1^T \rho_1 + \delta_i^{(s)} + \delta_i^2 - \delta_1^{(s)} - \delta_1^2, \quad (14)$$

so we transform it again below to eliminate this nonlinearity.

Subtracting squared range observations by reference is also useful and gives

$$r_i^2 - r_1^2 = -2\hat{\ell}^T (\rho_i - \rho_1) + \rho_i^T \rho_i - \rho_1^T \rho_1 + \epsilon_i^{(s)} + \epsilon_i^2 - \epsilon_1^{(s)} - \epsilon_1^2. \quad (15)$$

3.4 Double-Differencing by Epoch

In multi-epoch settings, we eliminate the nonlinearity in the differenced squared phase constraints by differencing again, this time by epoch. Using the notation of Equation (4) in Equation (14), we have

$$\lambda^2 \left((\dot{n}_i + \varphi_{i,j})^2 - (\dot{n}_1 + \varphi_{1,j})^2 \right) = -2\dot{\ell}_j^T (\rho_{i,j} - \rho_{1,j}) + \rho_{i,j}^T \rho_{i,j} - \rho_{1,j}^T \rho_{1,j} + \delta_{i,j}^{(s)} + \delta_{i,j}^2 - \delta_{1,j}^{(s)} - \delta_{1,j}^2 .$$

Subtracting the corresponding equation for epoch $j' \neq j$ eliminates the squared \dot{n}_i s from the left-hand side. Consider $(\dot{n}_i + \varphi_{i,j})^2 - (\dot{n}_i + \varphi_{i,j'})^2$,

$$\begin{aligned} (\dot{n}_i + \varphi_{i,j})^2 - (\dot{n}_i + \varphi_{i,j'})^2 &= (\varphi_{i,j}^2 + 2\varphi_{i,j}\dot{n}_i + \dot{n}_i^2) - (\varphi_{i,j'}^2 + 2\varphi_{i,j'}\dot{n}_i + \dot{n}_i^2) \\ &= (\varphi_{i,j}^2 - \varphi_{i,j'}^2) + 2(\varphi_{i,j} - \varphi_{i,j'})\dot{n}_i . \end{aligned}$$

The double-differenced constraints are

$$\begin{aligned} (\varphi_{i,j}^2 - \varphi_{i,j'}^2) + 2(\varphi_{i,j} - \varphi_{i,j'})\dot{n}_i \\ - (\varphi_{1,j}^2 - \varphi_{1,j'}^2) - 2(\varphi_{1,j} - \varphi_{1,j'})\dot{n}_1 &= -2\dot{\ell}_j^T (\rho_{i,j} - \rho_{1,j}) + \rho_{i,j}^T \rho_{i,j} - \rho_{1,j}^T \rho_{1,j} + \delta_{i,j}^{(s)} + \delta_{i,j}^2 - \delta_{1,j}^{(s)} - \delta_{1,j}^2 \\ &\quad + 2\dot{\ell}_{j'}^T (\rho_{i,j'} - \rho_{1,j'}) - \rho_{i,j'}^T \rho_{i,j'} + \rho_{1,j'}^T \rho_{1,j'} - \delta_{i,j'}^{(s)} - \delta_{i,j'}^2 + \delta_{1,j'}^{(s)} + \delta_{1,j'}^2 . \end{aligned}$$

These constraints are linear in $\dot{\ell}_j$, $\dot{\ell}_{j'}$, and the \dot{n}_i s.

When both the target and the references move between epochs, we use these constraints as is. When the target and/or the references are stationary, the constraints simplify. When the target is stationary so $\dot{\ell}_j = \dot{\ell}_{j'} = \dot{\ell}$ but the references move, we substitute on the right-hand side

$$-2\dot{\ell}_j^T (\rho_{i,j} - \rho_{1,j}) + 2\dot{\ell}_{j'}^T (\rho_{i,j'} - \rho_{1,j'}) = -2\dot{\ell}^T (\rho_{i,j} - \rho_{1,j} - \rho_{i,j'} + \rho_{1,j'}) .$$

When the target is moving but the references are stationary $\rho_{i,j} = \rho_{i,j'}$, we substitute on the right-hand side

$$-2\dot{\ell}_j^T (\rho_{i,j} - \rho_{1,j}) + \rho_{i,j}^T \rho_{i,j} - \rho_{1,j}^T \rho_{1,j} + 2\dot{\ell}_{j'}^T (\rho_{i,j'} - \rho_{1,j'}) - \rho_{i,j'}^T \rho_{i,j'} + \rho_{1,j'}^T \rho_{1,j'} = -2(\dot{\ell}_j - \dot{\ell}_{j'})^T (\rho_i - \rho_1) .$$

Incorporate the resulting constraints into a minimization problem allows us to estimate $\dot{\ell}_j - \dot{\ell}_{j'}$ but not $\dot{\ell}_j$ or $\dot{\ell}_{j'}$. We can overcome this problem because the minimization problem does allow us to estimate the \dot{n}_i s, which we can then substitute in the original phase constraints and estimate $\dot{\ell}_j$ and $\dot{\ell}_{j'}$ (separately).

When both the target and the references are stationary, the differencing leaves only error terms,

$$\begin{aligned} (\varphi_{i,j}^2 - \varphi_{i,j'}^2) + 2(\varphi_{i,j} - \varphi_{i,j'})\dot{n}_i \\ - (\varphi_{1,j}^2 - \varphi_{1,j'}^2) - 2(\varphi_{1,j} - \varphi_{1,j'})\dot{n}_1 &= +\delta_{i,j}^{(s)} + \delta_{i,j}^2 - \delta_{1,j}^{(s)} - \delta_{1,j}^2 \\ &\quad - \delta_{i,j'}^{(s)} - \delta_{i,j'}^2 + \delta_{1,j'}^{(s)} + \delta_{1,j'}^2 . \end{aligned}$$

This is not a useful constraint; in this case we use the two single-epoch constraints without subtracting them.

3.5 Linearizing Euclidean Distances

Finally, we can linearize the term $\|\ell - \rho_i\|_2$ that is present in both the range and phase constraints around an approximate location estimate ℓ_0 , which we can obtain by minimizing the residual of the range constraints alone. The Taylor-series approximation of the range near ℓ_0 is

$$\|\ell - \rho_i\|_2 = \|\ell_0 - \rho_i\|_2 + \frac{\partial \|\ell - \rho_i\|_2}{\partial \ell} (\ell - \ell_0) + \eta_i , \quad (16)$$

where gradient $\partial \|\ell - \rho_i\| / \partial \ell$ is evaluated at ℓ_0 and where $\eta_i = O(\|\ell - \ell_0\|^2)$ is a truncation error. The symbolic form of the gradient is

$$\frac{\partial \|\ell - \rho_i\|_2}{\partial \ell} = \frac{(\ell - \rho_i)^T}{\|\ell - \rho_i\|_2}$$

so its value at ℓ_0 is $(\ell_0 - \rho_i)^T / \|\ell_0 - \rho_i\|$.

The linear approximation gives us range and phase constraints that are linear in both $\mathring{\ell}$ and \mathring{n}_i , but with a large truncation error at short ranges:

$$\begin{aligned} r_i &= \|\ell_0 - \rho_i\|_2 + \frac{(\ell_0 - \rho_i)^T}{\|\ell_0 - \rho_i\|_2} (\mathring{\ell} - \ell_0) + \eta_i + \epsilon_i \\ \lambda\varphi_i + \lambda\mathring{n}_i &= \|\ell_0 - \rho_i\|_2 + \frac{(\ell_0 - \rho_i)^T}{\|\ell_0 - \rho_i\|_2} (\mathring{\ell} - \mathring{\ell}_0) + \eta_i + \delta_i. \end{aligned}$$

3.6 Linearizing Squared Phase Constraints

Finally, we also show how to linearize squared phase constraints, in order to obtain one constraint that is linear in both $\mathring{\ell}$ and \mathring{s}_i . We start from Equation (9),

$$\lambda^2 \mathring{s}_i = \left\| \mathring{\ell} - \rho_i \right\|_2^2 + \delta_i^{(s)} + \delta_i^2.$$

In principle we can use a Taylor-series approximation again, but since $\|\mathring{\ell} - \rho_i\|^2$ is a simple quadratic form in $\mathring{\ell}$, we can use a simpler algebraic approach:

$$\left\| \mathring{\ell} - \rho_i \right\|_2^2 = \left\| \mathring{\ell} - \ell_0 + \ell_0 - \rho_i \right\|_2^2 = \|\ell_0 - \rho_i\|_2^2 + 2(\ell_0 - \rho_i)^T (\mathring{\ell} - \ell_0) + \left\| \mathring{\ell} - \ell_0 \right\|_2^2.$$

We approximate the squared range using the first two terms on the right hand side, and we treat the last term as a truncation error $\eta^{(s)} = \|\mathring{\ell} - \ell_0\|^2$, which is independent of i . This gives us the linear constraint

$$\lambda^2 \mathring{s}_i = \|\ell_0 - \rho_i\|_2^2 + 2(\ell_0 - \rho_i)^T (\mathring{\ell} - \ell_0) + \eta^{(s)} + \delta_i^{(s)} + \delta_i^2. \quad (17)$$

4 Assembling Minimization Problems

We estimate the \mathring{n}_i s and the location $\mathring{\ell}$ (or $\mathring{\ell}_j$ s) by assembling constraints presented in Section 3 into residual minimization problems.

4.1 Single-Epoch Minimization Problems

In single-epoch settings, we assemble a minimization problem from $m - 1$ differenced squared phase constraints (13)

$$\lambda^2 \mathring{s}_i - \lambda^2 \mathring{s}_1 = -2\mathring{\ell}^T (\rho_i - \rho_1) + \rho_i^T \rho_i - \rho_1^T \rho_1 + \delta_i^{(s)} + \delta_i^2 - \delta_1^{(s)} - \delta_1^2$$

(recall that m is the number of references). We also add the linearized squared constraint for reference 1 from Equation (17),

$$\lambda^2 \mathring{s}_1 = \|\ell_0 - \rho_1\|_2^2 + 2(\ell_0 - \rho_1)^T (\mathring{\ell} - \ell_0) + \eta^{(s)} + \delta_1^{(s)} + \delta_1^2.$$

Next, we add $m - 1$ differenced squared range constraints from Equation (15),

$$r_i^2 - r_1^2 = -2\mathring{\ell}^T (\rho_i - \rho_1) + \rho_i^T \rho_i - \rho_1^T \rho_1 + \epsilon_i^{(s)} + \epsilon_i^2 - \epsilon_1^{(s)} - \epsilon_1^2$$

as well as m linearized range constraints

$$r_i = \|\ell_0 - \rho_i\|_2 + \frac{(\ell_0 - \rho_i)^T}{\|\ell_0 - \rho_i\|_2} (\mathring{\ell} - \ell_0) + \eta_i + \epsilon_i.$$

The last two families use each range constraint twice, once in each family. We use both families because their error terms are completely different.

4.2 Multiple-Epoch Minimization Problems

In the multiple-epoch settings, we start from the double-differenced squared phase constraints described in Section 3.4

$$\begin{aligned} & (\varphi_{i,j}^2 - \varphi_{i,j'}^2) + 2(\varphi_{i,j} - \varphi_{i,j'}) \dot{n}_i \\ - (\varphi_{1,j}^2 - \varphi_{1,j'}^2) - 2(\varphi_{1,j} - \varphi_{1,j'}) \dot{n}_1 &= -2\dot{\ell}_j^T(\rho_{i,j} - \rho_{1,j}) + \rho_{i,j}^T \rho_{i,j} - \rho_{1,j}^T \rho_{1,j} + \delta_{i,j}^{(s)} + \delta_{i,j}^2 - \delta_{1,j}^{(s)} - \delta_{1,j}^2 \\ & \quad + 2\dot{\ell}_{j'}^T(\rho_{i,j'} - \rho_{1,j'}) - \rho_{i,j'}^T \rho_{i,j'} + \rho_{1,j'}^T \rho_{1,j'} - \delta_{i,j'}^{(s)} - \delta_{i,j'}^2 + \delta_{1,j'}^{(s)} + \delta_{1,j'}^2, \end{aligned}$$

or their simplified variants when either the target or the references are stationary. For the case of two epochs, this gives $m - 1$ constraints.

We add the single-differenced range constraints from Equation (15),

$$r_{i,j}^2 - r_{1,j}^2 = -2\dot{\ell}_j^T(\rho_{i,j} - \rho_{1,j}) + \rho_{i,j}^T \rho_{i,j} - \rho_{1,j}^T \rho_{1,j} + \epsilon_{i,j}^{(s)} + \epsilon_{i,j}^2 - \epsilon_{1,j}^{(s)} - \epsilon_{1,j}^2.$$

In our implementation described below in Section 8, we currently add differences of these constraints by epoch, but one may consider adding them without double differencing.

Finally, we add the linearized phase and range constraints described in Section 3.5,

$$\begin{aligned} r_{i,j} &= \|\ell_{0,j} - \rho_{i,j}\|_2 + \frac{(\ell_{0,j} - \rho_{i,j})^T}{\|\ell_{0,j} - \rho_{i,j}\|_2} (\dot{\ell}_j - \ell_{0,j}) + \eta_{i,j} + \epsilon_{i,j} \\ \lambda\varphi_{i,j} + \lambda\dot{n}_i &= \|\ell_{0,j} - \rho_{i,j}\|_2 + \frac{(\ell_{0,j} - \rho_{i,j})^T}{\|\ell_{0,j} - \rho_{i,j}\|_2} (\dot{\ell}_j - \ell_{0,j}) + \eta_{i,j} + \delta_{i,j} \end{aligned}$$

(again for both epochs j and j').

4.3 Linearize-First Minimization Problems (LAMBDA)

For reference and to specify precisely the LAMBDA algorithm that we used in the numerical experiments below, we specify the constraints that are used in our implementation of the LAMBDA method. Specifically, in this method we assemble the linearized phase and range constraints described in Section 3.5,

$$\begin{aligned} r_{i,j} &= \|\ell_{0,j} - \rho_{i,j}\|_2 + \frac{(\ell_{0,j} - \rho_{i,j})^T}{\|\ell_{0,j} - \rho_{i,j}\|_2} (\dot{\ell}_j - \ell_{0,j}) + \eta_{i,j} + \epsilon_{i,j} \\ \lambda\varphi_{i,j} + \lambda\dot{n}_i &= \|\ell_{0,j} - \rho_{i,j}\|_2 + \frac{(\ell_{0,j} - \rho_{i,j})^T}{\|\ell_{0,j} - \rho_{i,j}\|_2} (\dot{\ell}_j - \ell_{0,j}) + \eta_{i,j} + \delta_{i,j} \end{aligned}$$

(for a single or multiple epochs, always with a single set of n_i s).

4.4 From Sets of Constraints to Generalized Least Squares

In the single-epoch case, we end up with a set of constraints of the form

$$A\dot{\ell} + B\dot{s} - d = e$$

where A is a known matrix, B is a known matrix, d is a known vector, and e is a vector of error terms. The unknown parameters are the 2D or 3D location vector $\dot{\ell}$ and the m -vector \dot{s} of discrete parameters of the form $\dot{s}_i = (\varphi_i + \dot{n}_i)^2$ where $\dot{n}_i \in \mathbb{N}$. In the multi-epoch case, we end up with a set of constraints of the form

$$A\dot{\ell} + B\dot{n} - d = e$$

where $\dot{n} \in \mathbb{N}^m$.

In both cases, some of the rows of B are identically zero. These rows corresponds to constraints that were derived from range observations alone and are independent of any phase observations.

Estimating the unknown vectors well requires a characterization of the statistical and/or mathematical properties of the error vectors e . Without loss of generality, one can assume that the expected value of the e_i s is zero, because

if some have a nonzero expectation that can be computed or estimated, the expectation should be subtracted from d , leaving an error vector with approximately zero expectation. That is, we rearrange our equations as

$$A\hat{\ell} + B\hat{s} - (d + \text{expectation}(e)) = e - \text{expectation}(e).$$

We estimate $\hat{\ell}$ and \hat{s} or \hat{n} by minimizing $\|W(e - \text{expectation}(e))\|_2$ where W is a weight matrix that is an inverse factor of an approximate covariance matrix $C = (W^T W)^{-1}$. We stress that in general, the accuracy of the estimate depends only weakly on the accuracy of W . Relative accuracy to within 1% or even just 10% is usually sufficient, and higher accuracy of W does not improve much the accuracy of the estimates.

We minimize the two-norm of $e - \text{expectation}(e)$ because this is computationally easier than minimizing other norms, and because when e is distributed normally with a known expectation and a known covariance matrix C , the two-norm minimizers are also the maximum-likelihood estimators.

However, in our case some elements of e are not distributed normally, not even approximately. This requires deeper insights on the choice of C and on the implications of this choice. Many years of experience with LAMBDA applied to GNSS problems yielded the following insights, which are also relevant to our problem (Toledo 2020):

The set of phase observations have many local minima, including one at the true \hat{n} and near $\hat{\ell}$, but typically many more, especially when the number m of references is small. The residual at some of the other locations may be similar or even smaller than at the true location, making it impossible to identify the correct location from these constraints alone. The range (or ToA) constraints help identify the correct solution. Far from the true solution, these constraints have large residuals, which eliminates these hypothetical solutions even if the residual of the phase constraints alone there is tiny.

Therefore, correctly weighing the phase constraints is key to the accuracy of the estimates. If these are incorrectly weighed with respect to one another, or too weakly weighed relative to the range/ToA observations, the minimizer tends to remain near the true location, but its accuracy suffers. On the other hand, if the range/ToA constraints are weighed too weakly, the likelihood that the minimizer is not at all near the true solution increases; but if the minimizer happens to be near the true solution, the weak weighing of the range/ToA constraints has little effect on the accuracy of the estimate.

These insights inform our analyses of the error terms in the next section.

5 The Distribution of the Error Terms and Approximations of Their Covariance Matrices

We now analyze each error term introduced in Section 3, aiming to characterize their distribution. In particular, we aim to estimate their expectation and their variance, or at least bound their variance, in order to subtract the approximate expectation from d and to correctly weigh the constraints.

We assume that the observation errors ϵ_i and δ_i are Gaussian, uncorrelated, and have zero mean and known standard deviations specified in Section 2.1.

5.1 Squares of Observation Errors

In constraints that are based on squaring, we have ϵ_i^2 or δ_i^2 terms. Their distribution is scaled $\chi^2(1)$ with expectation $\sigma^2(\epsilon_i)$ or $\sigma^2(\delta_i)$ and standard deviation $\sqrt{2}\sigma^2(\epsilon_i)$ or $\sqrt{2}\sigma^2(\delta_i)$.

We assume that these terms can be neglected. The δ_i^2 errors are tiny, and the ϵ_i^2 are also small and shadowed by larger errors.

5.2 The Errors $\epsilon_i^{(s)}$ and $\delta_i^{(s)}$

The errors

$$\begin{aligned}\delta_i^{(s)} &= 2\delta_i\|\hat{\ell} - \rho_i\| \\ \epsilon_i^{(s)} &= 2\epsilon_i\|\hat{\ell} - \rho_i\|\end{aligned}$$

are scaling of ϵ_i and δ_i , since the norm $\|\hat{\ell} - \rho_i\|$ is deterministic, even though it is not known. Therefore, their expectation is zero, and their standard deviations are $2\sigma(\epsilon_i)\|\hat{\ell} - \rho_i\|$ and $2\sigma(\delta_i)\|\hat{\ell} - \rho_i\|$. We do not know the precise

value of $\|\dot{\ell} - \rho_i\|$, but we can approximate the the standard deviations with

$$\begin{aligned}\bar{\sigma}\left(\delta_i^{(s)}\right) &= 2\delta_i\|\ell_0 - \rho_i\| \\ \bar{\sigma}\left(\epsilon_i^{(s)}\right) &= 2\epsilon_i\|\ell_0 - \rho_i\|.\end{aligned}$$

For the purpose of weighing the constraints, this is an excellent approximation.

These errors are uncorrelated with each other, due to our assumption that the ϵ_i s and δ_i s, but they are correlated with some of the other error terms in the same constraints.

5.3 Linearization Errors of Squared Ranges

If we assume that $\dot{\ell} - \ell_0$ is Gaussian, has zero expectation, and has covariance matrix C_0 , then the linearization error $\eta^{(s)} = \|\dot{\ell} - \ell_0\|^2$ is a generalized χ^2 random variable whose expectation is $\text{trace}(C_0)$ and whose variance is $2\|C_0\|_F^2$ (twice the Frobenius norm of C_0). Note that

$$\text{trace}(C_0)/\sqrt{2} \leq \sqrt{2}\|C_0\|_F \leq \sqrt{2}\text{trace}(C_0). \quad (18)$$

We weigh the squared range constraint as if $\eta^{(s)}$ is distributed normally with zero expectation and with variance $\|C_0\|_F^2$.

We now prove (18).

Lemma 1. *Let C_0 be a 2-by-2 or 3-by-3 symmetric semidefinite matrix. Then*

$$\text{trace}(C_0)/\sqrt{2} \leq \sqrt{2}\|C_0\|_F \leq \sqrt{2}\text{trace}(C_0).$$

Proof. Let $0 \leq v_1, \dots, v_d$ be the eigenvalues of C_0 . We have

$$\begin{aligned}\|C_0\|_F &= \sqrt{\sum_i v_i^2} = \|v\|_2 \\ \text{trace}(C_0) &= \sum_i v_i = \|v\|_1.\end{aligned}$$

The upper bound on $\sqrt{2}\|C_0\|_F$ holds because $\|v\|_2 \leq \|v\|_1$ for any vector v . The lower bound holds for dimensions $d = 1, 2, 3, 4$ because $\|v\|_1 \leq \sqrt{d}\|v\|_2$ (Bernstein 2005, Fact 9.8.10). \square

5.4 Errors in Linearization of Ranges

We now analyze the error in the linearization of ranges. We have

$$\begin{aligned}\left\|\dot{\ell} - \rho_i\right\|_2 &= \|\ell_0 - \rho_i\|_2 + \frac{\partial\|\ell - \rho_i\|_2}{\partial\ell}\left(\dot{\ell} - \ell_0\right) + \eta_i \\ &= \|\ell_0 - \rho_i\|_2 + \frac{(\ell_0 - \rho_i)^T}{\|\ell_0 - \rho_i\|_2}\left(\dot{\ell} - \ell_0\right) + \eta_i\end{aligned}$$

(recall that the derivative is evaluated at ℓ_0). Therefore, the error term that we need to analyze is

$$\begin{aligned}\eta_i &= \left\|\dot{\ell} - \rho_i\right\|_2 - \|\ell_0 - \rho_i\|_2 - \frac{(\ell_0 - \rho_i)^T}{\|\ell_0 - \rho_i\|_2}\left(\dot{\ell} - \ell_0\right) \\ &= \left\|\dot{\ell} - \rho_i\right\|_2 - \|\ell_0 - \rho_i\|_2 - \left\|\dot{\ell} - \ell_0\right\|_2 \frac{(\ell_0 - \rho_i)^T}{\|\ell_0 - \rho_i\|_2} \frac{\left(\dot{\ell} - \ell_0\right)}{\left\|\dot{\ell} - \ell_0\right\|_2} \\ &= \left\|\dot{\ell} - \rho_i\right\|_2 - \|\ell_0 - \rho_i\|_2 - \left\|\dot{\ell} - \ell_0\right\|_2 \cos(\pi - \alpha).\end{aligned}$$

where α is the angle between the line segments $\ell_0 \leftrightarrow \dot{\ell}$ and $\ell_0 \leftrightarrow \rho_i$, as shown in Figure 1 (top).

When ρ_i , ℓ_0 , and $\dot{\ell}$ are collinear, the approximation is exact; either $\alpha = \pi$ and $\cos(\pi - \alpha) = 1$ and

$$\left\|\dot{\ell} - \rho_i\right\|_2 = \|\ell_0 - \rho_i\|_2 + \left\|\dot{\ell} - \ell_0\right\|_2,$$

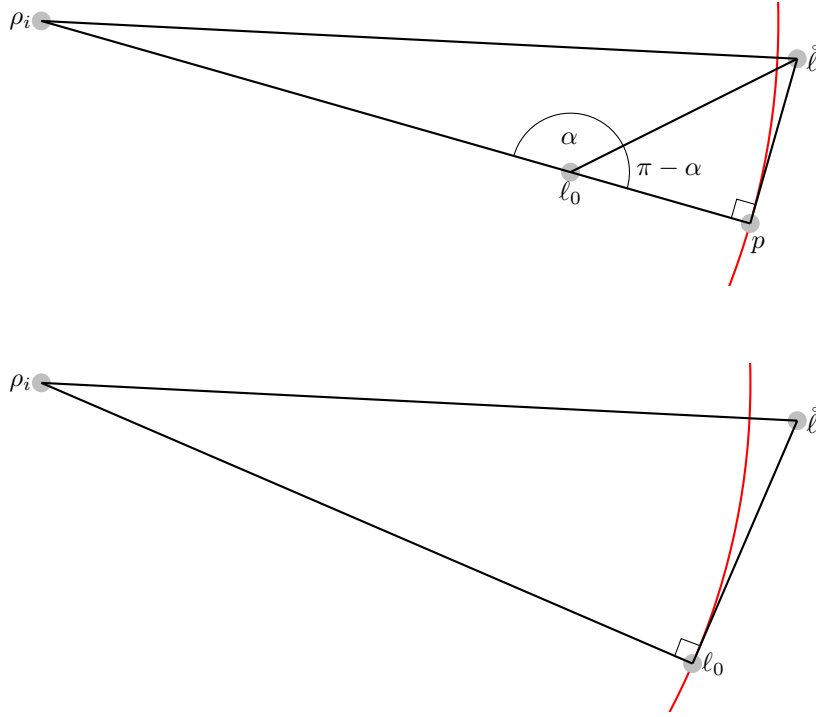


Figure 1: Top: The distance between ρ_i and the red circle (equal to $\|\rho_i - p\|$) is the linear approximation to $\|\rho_i - \hat{\ell}\|$. Note that $\|\ell_0 - p\| = \|\ell_0 - \hat{\ell}\| \cos(\pi - \alpha)$. Bottom: the worst-case linearization error, when $\alpha = \pi/2$. Note that the distances $\|\ell_0 - \hat{\ell}\|$ is the same at the top and at the bottom, as are the coordinates of ρ_i and $\hat{\ell}$.

or $\alpha = 0$, $\cos(\pi - \alpha) = -1$, and

$$\left\| \hat{\ell} - \rho_i \right\|_2 = \|\ell_0 - \rho_i\|_2 - \left\| \hat{\ell} - \ell_0 \right\|_2 .$$

In both cases we have $\eta_i = 0$. The error is largest when $\alpha = \pi/2$ and $\cos(\pi - \alpha) = 0$, so the approximation is $\|\ell_0 - \rho_i\|_2$ with no correction, as shown in the bottom drawing in Figure 1. The magnitude of the linearization error in this case is

$$\left\| \hat{\ell} - \rho_i \right\|_2 - \|\ell_0 - \rho_i\|_2 ,$$

the difference between the hypotenuse of the right triangle $\rho_i \leftrightarrow \ell_0 \leftrightarrow \hat{\ell}$ and the leg $\rho_i \leftrightarrow \ell_0$ of that triangle. If we denote the length long leg of the triangle $r = \|\ell_0 - \rho_i\|$ and the short leg $d = \left\| \hat{\ell} - \ell_0 \right\|$, the error is

$$\sqrt{r^2 + d^2} - r .$$

We now estimate the magnitude of this expression for d much smaller than r . We define $f(d) = \sqrt{r^2 + d^2}$ and differentiate

$$\begin{aligned} \frac{\partial f}{\partial d} &= \frac{d}{\sqrt{r^2 + d^2}} \\ \frac{\partial^2 f}{\partial d^2} &= \frac{r^2}{(r^2 + d^2)^{3/2}} . \end{aligned}$$

Constraint	Notation	Distribution	Approximation
range observations (1)	ϵ_i	$\mathcal{N}(0, \sigma^2(\epsilon_i))$	
carrier-phase observations (2)	δ_i	$\mathcal{N}(0, \sigma^2(\delta_i))$	
initial location estimate	$\mathring{\ell} - \ell_0$	$\mathcal{N}(0, C_0)$	
squared range observations (10)	ϵ_i^2	$\chi_1^2(\sigma^2(\epsilon_i), 2\sigma^4(\epsilon_i))$	0
squared range observations (10)	$\epsilon_i^{(s)} = 2\epsilon_i \ \mathring{\ell} - \rho_i\ $	$\mathcal{N}(0, 2\epsilon_i \ \mathring{\ell} - \rho_i\)$	$\mathcal{N}(0, 2\epsilon_i \ \ell_0 - \rho_i\)$
squared phase observations (7)	δ_i^2	$\chi_1^2(\sigma^2(\delta_i), 2\sigma^4(\delta_i))$	0
squared phase observations (7)	$\epsilon_i^{(s)} = 2\delta_i \ \mathring{\ell} - \rho_i\ $	$\mathcal{N}(0, 2\delta_i \ \mathring{\ell} - \rho_i\)$	$\mathcal{N}(0, 2\delta_i \ \ell_0 - \rho_i\)$
linearized squared ranges (17)	$\eta^{(s)} = \ \mathring{\ell} - \ell_0\ ^2$	$\chi_1^2(\text{trace}(C_0), 2\ C_0\ _F^2)$	$\mathcal{N}(0, \text{trace}(C_0))$
linearized ranges (16)	$\eta_i \lesssim \eta^{(s)} / (2\ \ell_0 - \rho_i\)$	—	$\mathcal{N}(0, \text{trace}(C_0)/100\ \ell_0 - \rho_i\)$

Table 1: Notation and distributions of the error terms in the original constraints (top three rows) and in derived constraints (bottom six). We have not fully characterized the distribution of η_i in the bottom row, so we show a bound on the error, not a distribution; the \lesssim signifies that the bound is a second-order Taylor approximation, not an exact bound.

We approximate f for small d (relative to a large r) using its Taylor series, evaluating the derivatives at $d = 0$,

$$\begin{aligned}
f(d) &= \sqrt{r^2 + d^2} \\
&= f(0) + \frac{\partial f}{\partial d}d + \frac{1}{2}\frac{\partial^2 f}{\partial d^2}d^2 + O(d^3) \\
&\approx f(0) + \frac{\partial f}{\partial d}d + \frac{1}{2}\frac{\partial^2 f}{\partial d^2}d^2 \\
&= r + \frac{0}{r}d + \frac{1}{2}\frac{1}{r}d^2 \\
&= r + \frac{1}{2}\frac{d^2}{r}.
\end{aligned}$$

This shows that the linear approximation of the worst-case error, for a large range r and a small displacement d , behaves like

$$\frac{1}{2}\frac{d^2}{r}.$$

The denominator $r = \|\ell_0 - \rho_i\|$ is deterministic, not random, so the bound itself is a scaling of $d^2 = \|\mathring{\ell} - \ell_0\|^2 = \eta_i^{(s)}$, a generalized χ^2 random variable whose expectation and variance are $\text{trace}(C_0)$ and $2\|C_0\|_F^2$. The scaling factor is $1/(2r) = 1/(2\|\ell_0 - \rho_i\|)$.

The distribution of η_i , as opposed to this upper bound, also depends on α and we do not attempt to fully characterize it.

Figure 2 presents the statistics of η_i for a simple normal distribution of $\mathring{\ell} - \ell_0$. We see that the mean error is about twice the value of

$$\frac{1}{2}\frac{\text{trace}(C_0)}{\|\ell_0 - \rho_i\|},$$

and that the maximum error over one million experiments is much higher.

In our algorithms, we weigh each linearized constraint

$$\left(\frac{1}{100}\frac{\text{trace}(C_0)}{\|\ell_0 - \rho_i\|}\right)^{-1},$$

which works well in simulations, in spite of the somewhat high weights that the 1/100 factor induces. The η_i s are correlated because of their shared dependence on $\|\mathring{\ell} - \ell_0\|$, and because the relations between the α s are a function of the location of the references, but we do not model these correlations in the weighing matrix.

5.5 Overall Approximate Covariance Matrices

Table 1 lists all the error terms in our constraints, our characterization of the distribution of each error (or an upper bound for the one term for which we do not have a complete characterization), and the approximations of the expectation and variance of the errors that we use to weigh the constraints.

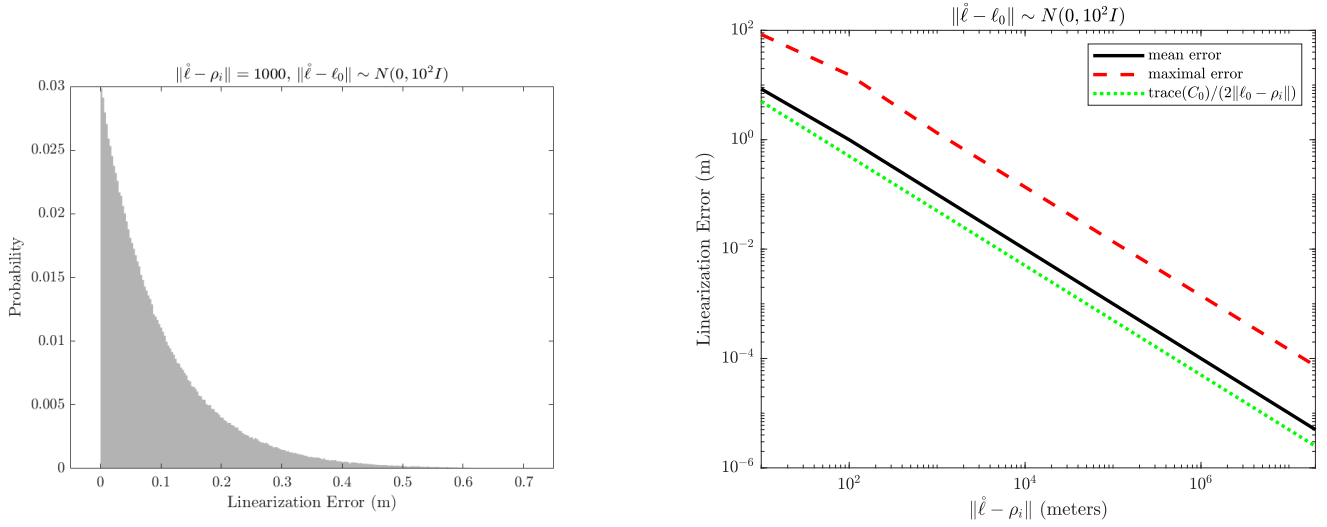


Figure 2: The distribution and mean of linearization errors when $\ell - \ell_0$ is distributed normally with zero expectation and covariance $10^2 I$, in three dimensions. The histogram on the left shows the distribution of errors in 1,000,000 experiments, when the target is a kilometer from the target, $\|\hat{\ell} - \rho_i\| = 1000$. The value of $(1/2)\text{trace}(C_0) / \|\ell_0 - \rho_i\|$ is about 0.05. The graph on the right shows the mean error, maximal error, and the bound $(1/2)\text{trace}(C_0) / \|\ell_0 - \rho_i\|$ for a whole spectrum of ranges $\|\hat{\ell} - \rho_i\|$.

By our assumptions, the ϵ_i s and the δ_i s are mutually independent, so they are uncorrelated. The squares ϵ_i^2 and δ_i^2 are statistically dependent on ϵ_i and δ_i , respectively, but are uncorrelated with them. The error in the initial location $\hat{\ell} - \ell_0$ depends on the ϵ_i s; it is possible to approximate the covariance of the error as a linear function of the ϵ_i s, but our implementation neglects this. The $\eta_i^{(s)}$ s and η_i s, which are functions of $\hat{\ell} - \ell_0$ also depends on the ϵ_i s; the dependence can be modeled but our implementation neglects it.

We, therefore, approximate the covariance matrix of the individual error terms

$$e_{\text{raw}} = \begin{bmatrix} \delta_1 \\ \vdots \\ \delta_m \\ \hline \delta_1^2 \\ \vdots \\ \delta_m^2 \\ \hline \epsilon_1 \\ \vdots \\ \epsilon_m \\ \hline \epsilon_1^2 \\ \vdots \\ \epsilon_m^2 \\ \hline \eta_1 \\ \vdots \\ \eta_m \\ \hline \eta^{(s)} \end{bmatrix}$$

up with a generalized least squares problem of the form

$$\hat{\ell}, \hat{s} = \arg \min_{\ell, s} \|W (A\ell + Bs - d)\|_2, \quad s_i = (n_i + \varphi_i)^2 \text{ where } n_i \in \mathbb{N},$$

and in multi-epoch case, we end up with

$$\hat{\ell}, \hat{n} = \arg \min_{\ell, n} \|W (A\ell + Bn - d)\|_2, \quad n_i \in \mathbb{N}.$$

In both cases, W , A , and B are known matrices and d is a known vector.

In both cases the vector whose norm we minimize is linear in ℓ and s (or ℓ and n) and in both cases we have both real unknown parameters ℓ and discrete unknown parameters, s or n . In both cases the first step is identical: we use an orthogonal projection to eliminate the real parameters ℓ . Let U be an orthonormal basis for the column space of WA . We can compute U using the singular value decomposition (SVD), or somewhat more cheaply, using a QR factorization. It is well known and easy to see that

$$\begin{aligned} \hat{s} &= \arg \min_{\ell, s} \|W (A\ell + Bs - d)\|_2 \\ &= \arg \min_s \|(I - UU^T) (Bs - d)\|_2. \end{aligned}$$

We now have a least-squares problem with discrete (or integer) parameters only, typically over determined.

Next, we transform the problem so that the coefficient matrix is triangular and square.

We compute the QR factorization of $(I - UU^T)B = QR$, where Q is orthonormal with m columns and R is square and upper triangular. Multiplying the residual by Q^T preserves its norm, so,

$$\begin{aligned} \hat{s} &= \arg \min_s \|(I - UU^T) (Bs - d)\|_2 \\ &= \arg \min_s \|Rs - Q^T (I - UU^T) d\|_2. \end{aligned} \tag{19}$$

Least squares problems of the form (19) with integer parameters are NP hard (Agrell et al. 2002; Micciancio 2001; Emde Boas 1981) and hard to approximate (Dinur et al. 2003), but they are routinely solved exactly in RTK using a three-phase approach. In the first phase, the LLL algorithm (Lenstra, Lenstra, and Lovász 1982) or one of its variants (Luk and Tracy 2008; Luk and Qiao 2011) applies a series of unimodular transformations to the columns of R , transforming (19) into

$$\hat{s} = \arg \min_{\tilde{s}} \|(RG) (G^{-1}\tilde{s}) - Q^T (I - UU^T) d\|_2 = G \arg \min_{\tilde{s}} \|(RG) (G^{-1}\tilde{s}) - Q^T (I - UU^T) d\|_2,$$

where RG retains the square upper-triangular form. In the second phase, a specialized branch-and-bound algorithm, called the Schnorr-Euchner search (Schnorr and Euchner 1994) finds the minimizer of the unimodularly-transformed problem. In the last phase, G is applied to the solution, to transform it into a minimizer of (19). The first phase is optional and its role is to heuristically reduce the cost of the search phase.

In the next subsections we explain how to adapt both the first and second phases to the case of discrete parameters that are not integers. We start with the second phase, since understanding it makes the role of the first easier to understand.

6.1 Adapting the Schnorr-Euchner Search to Shifted Squares

The Schnorr-Euchner search algorithm (Schnorr and Euchner 1994) performs a sequence of assignments to the unknown parameters, starting from the last, s_m , progressing backwards to s_{m-1} , s_{m-2} and up to s_1 , but backtracking when necessary. Backtracking allows the algorithm to try a different assignment to a parameter s_i that has already been assigned to. In the original algorithm, designed for integer least-squares problems, integers are assigned to the s_i s.

We modify the algorithm so that the set of values $s_{i,k}$ that we assign to s_i are not integers but rather numbers of the form $s_{i,k} = (n_{i,k} + \varphi_i)^2$ where $n_{i,k} \in \mathbb{N}$.

Backtracking in the Schnorr-Euchner search algorithm defines an implicit rooted tree, in which each level except for the root corresponds to a parameter s_i , each vertex to an assignment of s_i to a particular value $s_{i,k}$, and each path from a vertex $s_{i,k}$ to the root represents a concrete assignment to s_i, \dots, s_m . The abstract tree is infinite, with each vertex having an infinite number of children, but the Schnorr-Euchner search always terminates, so it explores a finite subtree. The algorithm explores the children of $s_{i+1,k}$, which represent a specific assignment of $s_{i+1:m}$, in a

particular order. This order is critical both to the correctness and to the efficiency of the algorithm. In particular, at $s_{i+1,k}$, the contribution of row i to the sum of squares is

$$(R_{i,i}s_i + R_{i,i+1:m}s_{i+1:m} - (Q^T(I - UU^T)d)_i)^2. \quad (20)$$

For the algorithm to work correctly and efficiently, these contributions must grow monotonically with each assignment to s_i . We denote

$$z_i = -\frac{R_{i,i+1:m}s_{i+1:m} - (Q^T d)_i}{R_{i,i}}.$$

When s_i is constrained to the set $(n_i + \varphi_i)^2$, $n_i \in \mathbb{N}$, the contribution of row i is proportional to

$$\left((n_i + \varphi_i)^2 - z_i \right)^2.$$

The square is monotone, so this expression is minimized when $|(n_i + \varphi_i)^2 - z_i|$ is minimized. We test both $\lfloor \sqrt{z_i} - \varphi_i \rfloor$ and $\lceil \sqrt{z_i} - \varphi_i \rceil$ and assign to $n_{i,1}$ the value n_1 that yields the smaller contribution. This is the equivalent of the so-called Babai rounding for this problem. Now suppose that we already tested integer values $n_1 - l$ to $n_1 + r$. The next largest contribution will be either at $n_1 - l - 1$ or $n_1 + r + 1$. We again test both and take the one that yields the smaller contribution.

We note that this adaptation is valid for any set of discrete values that we can enumerate in increasing distance from a real value z_i .

6.2 QR Decompositions with Column Pivoting

The Schnorr-Euchner search explores a smaller finite subtree of the infinite abstract tree when diagonal elements of R near the bottom right corner have large absolute values. When the parameters are integer-valued, applying the LLL algorithm or its variants to R often increases the absolute values of diagonal elements near the bottom-right, making the subsequent search more efficient. LLL and its variants apply a sequence of unimodular column operations to R in a way that preserves the upper-triangular structure. Unimodular transformations transform integer vectors to integer vectors, so the search can be applied to the transformed RG , and the minimizing integer vector $G^{-1}\hat{s}$ can be transformed back to an integer minimizer $\hat{s} = GG^{-1}\hat{s}$ of (19).

In the single-epoch case, we apply the Schnorr-Euchner search to sets of shifted squares, so we need G to preserve this property. Unimodular matrices do not necessarily preserve it. Therefore, we utilize a more restricted class of matrices, namely permutation matrices.

We explore two strategies for generating the permutation. Neither of them is new. The simpler strategy incorporates greedy column pivoting into the QR factorization that produces R , aiming to populate the diagonal of RG with large entries near the bottom. The pivoting selects the column with the smallest norm to be eliminated next. This is the exact opposite of the policy of column pivoting in numerical libraries, which has a different aim, to identify rank deficiency.

We also explore a more sophisticated strategy called V-BLAST (Damen, El Gamal, and Caire 2003; Chang and Paige 2007). Initially, algorithms to produce this permutation were asymptotically about as expensive as LLL (Damen, El Gamal, and Caire 2003), but variants that are asymptotically as efficient as the standard QR factorization have been developed (Chang and Paige 2007). The idea behind these algorithms is to greedily select columns from last to first, always selecting next the column that maximizes the next diagonal value in RG .

We report below on the efficacy of these optimizations.

7 Polynomial-Time Algorithms Using Geometric Arrangements

This section describes geometric algorithms to find the minimizer of (5) that run in polynomial time. We focus on single-epoch problems for simplicity.

7.1 Introduction to Arrangements

The algorithms that we present rely on a data structure called a *geometric arrangement* (Halperin and Sharir 2017) to decompose the 2- or 3-dimensional Euclidean space into cells, faces, and vertices. Consider a set of m error-free carrier-phase constraints

$$\lambda\varphi_i + \lambda\hat{n}_i = \left\| \hat{\ell} - \rho_i \right\|_2$$

where $\varphi_i \in [0, 1)$. The target lies outside or on the circle (or sphere in 3D) defined by all points ℓ satisfying

$$\lambda \hat{n}_i = \|\ell - \rho_i\|_2$$

and strictly inside the circle (sphere)

$$\lambda (\hat{n}_i + 1) = \|\ell - \rho_i\|_2 .$$

These two circles (spheres) already induce an arrangement that partitions the space into three cells and two faces or edges that separate them. The cells are the disk (or ball in 3D) $\|\ell - \rho_i\|_2 < \lambda \hat{n}_i$, the annulus $\lambda \hat{n}_i < \|\ell - \rho_i\|_2 < \lambda (\hat{n}_i + 1)$, and the unbounded region $\|\ell - \rho_i\|_2 > \lambda (\hat{n}_i + 1)$. The faces or edges are the two circles or spheres. Since the two circles/spheres do not intersect, there are no vertices in this arrangement.

Since we do not know the value of \hat{n}_i , algorithmically it makes sense to construct an arrangement induced by all the plausible circles/spheres whose center is ρ_i . We can derive a set of plausible n_i s from the range constraint (1)

$$r_i = \left\| \hat{\ell} - \rho_i \right\|_2 + \epsilon_i .$$

We define

$$\begin{aligned} \bar{n}_i &= \left\lceil \frac{\left\| \hat{\ell} - \rho_i \right\|_2 + c\sigma(\epsilon_i)}{\lambda} \right\rceil \approx \left\lceil \frac{r_i + c\sigma(\epsilon_i)}{\lambda} \right\rceil \\ \underline{n}_i &= \left\lfloor \frac{\left\| \hat{\ell} - \rho_i \right\|_2 - c\sigma(\epsilon_i)}{\lambda} \right\rfloor \approx \left\lfloor \frac{r_i - c\sigma(\epsilon_i)}{\lambda} \right\rfloor \end{aligned}$$

for some appropriate constant c , say 6, such that $\lambda \underline{n}_i < \|\hat{\ell} - \rho_i\| < \lambda \bar{n}_i$ with high probability. This arrangement has $E_i = \bar{n}_i - \underline{n}_i$ annuli cells. The target lies, with high probability, in one of them or on the circles that separate them.

Now consider another constraint specifying to carrier phase with respect to another reference i' . It will define $E_{i'} = \bar{n}_{i'} - \underline{n}_{i'}$ additional annuli defined by $\bar{n}_{i'} - \underline{n}_{i'} + 1$ circles. Each cell in the resulting arrangement corresponds to a particular value of n_i and a particular value of $n_{i'}$.

With m pairs of range and carrier-phase constraints, we have at most mE circles/spheres that define the annuli, where $E = \max_i E_i$. How many cells can we have in the arrangement? It turns out that the number is $O((mE)^2)$ in 2D and $O((mE)^3)$ in 3D and that the arrangement data structure can be constructed and its cells, faces, and vertices enumerated in time and space $O((mE)^2)$ in 2D and $O((mE)^3)$ in 3D. We need to qualify the statement that arrangements can be constructed efficiently. Algorithms that correctly enumerate the cells of arrangements of circles and spheres are complex (Halperin and Sharir 2017). Currently, there is an implementation of an algorithm that enumerates arrangements of circles (Fogel, Halperin, and Wein 2012) but not of spheres, even though the algorithm is known.

Each cell of the arrangement corresponds to a particular integer value for each unknown n_i . We refer to this integer vector as the *label* of the cell. Therefore, we can enumerate the cells, determine the label n of each one, and solve the real nonlinear least squares problem

$$\hat{\ell}(n) = \arg \min_{\ell} \left\| W \left(M(\ell) - \begin{bmatrix} 0 \\ \lambda I \end{bmatrix} n - \begin{bmatrix} r_i \\ \lambda \varphi_i \end{bmatrix} \right) \right\|_2 .$$

The assignment with the smallest residual defines the global solution to (5),

$$\hat{\ell}, \hat{n} = \arg \min_{\ell, n} \left\| W \left(M(\ell) - \begin{bmatrix} 0 \\ \lambda I \end{bmatrix} n - \begin{bmatrix} r_i \\ \lambda \varphi_i \end{bmatrix} \right) \right\|_2 .$$

(The cells in an arrangement are traditionally considered to be open sets, faces are semi-open, and vertices are closed; the assumption $\varphi_i \in [0, 1)$ essentially unifies each face and vertex with a particular cell, so that these unified cells form a partition of the admissible space.) The surprising aspect of this approach is that there are only $O((mE)^2)$ different integer assignments of n that are consistent with hypothetical target locations ℓ , even though each n_i can assume E_i different values. Enumerating all the possible assignments of all the n_i s would have generated $\prod_{i=0}^m E_i \approx E^m$, which is exponential in m . The arrangement of mE circles shows that there are only $O((mE)^2)$ geometrically-consistent assignments of m and it allows us to enumerate them efficiently.

Algorithm 1 A framework for geometric solvers of our generalized least-squares problems.

Construct a geometric arrangement of spheres (circles) induced by carrier-phase constraints

Enumerate the labels of the cells, faces, and vertices

For each integer-vector label n , solve

$$\hat{\ell}(n) = \arg \min_{\ell} \left\| W \left(M(\ell) - \begin{bmatrix} 0 \\ \lambda I \end{bmatrix} n - \begin{bmatrix} r_i \\ \lambda \varphi_i \end{bmatrix} \right) \right\|_2$$

and record the norm of the weighted residual.

Output the solution with the minimal weighted residual.

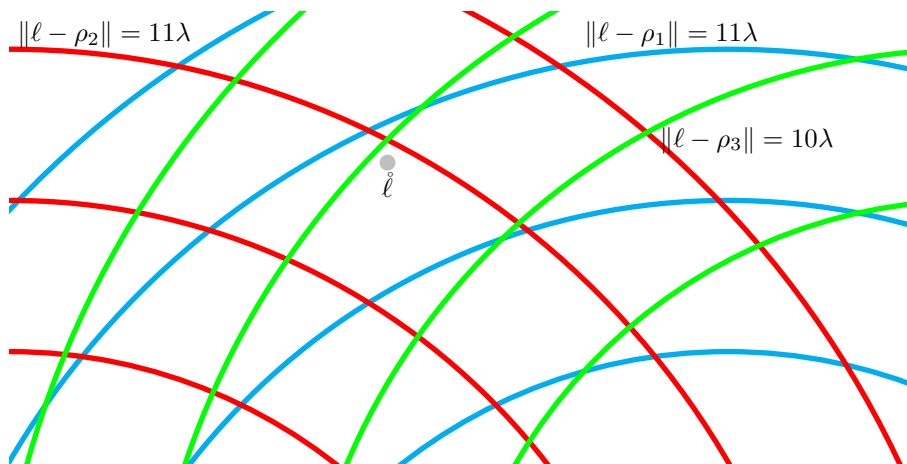


Figure 3: An illustration that demonstrates that the minimizing set of integers might not be the label of any cell in the arrangement. Circles with center ρ_1 are depicted in cyan, those with center ρ_2 in red, and those with ρ_3 in green. Suppose that $\delta_2 \leq 0$ and $\delta_3 \leq 0$, so that $\lambda\varphi_2 + \lambda \cdot 10 = \|\hat{\ell} - \rho_2\| + \delta_2$ and $\lambda\varphi_3 + \lambda \cdot 10 = \|\hat{\ell} - \rho_3\| + \delta_3$ with φ_2 and φ_3 both close to 1, but that $\delta_1 > 0$ is sufficiently large so that $\lambda\varphi_1 + \lambda \cdot 11 = \|\hat{\ell} - \rho_1\| + \delta_1$ with φ_1 is close to 0. The label of the cell containing $\hat{\ell}$ is $[10 \ 10 \ 10]$ but the minimizing integer vector is $[11 \ 10 \ 10]$, which is not the label of any cell.

In 3 dimensions, an arrangement of at most mE spheres define the geometrically-consistent assignments of n . The complexity of the arrangement and the time and space to construct is are $O((mE)^3)$.

So far, we have ignored an important aspect of our problem: our carrier-phase constraints are not exact but contain small additive errors δ_i . The next section shows that we must construct the arrangement in a way that tolerates these observation errors. We then describe several ways to construct arrangements that allow us to enumerate all the geometrically-consistent assignments of n in the presence of small errors in the carrier-phase constraints.

7.2 Observation Errors and Arrangements of Spheres with Integer Radii

Consider an arrangement of circles of the form

$$\lambda n_i = \|\ell - \rho_i\|_2 ,$$

which we refer to as an arrangement of spheres or circles with integer radii. Suppose that the target $\hat{\ell}$, which lies in a cell labeled \hat{n}_i , lies very close to its i th outer sphere $\hat{n}_i + 1$ and for which $\delta_i > 0$ is small but larger than the distance between $\hat{\ell}$ and that sphere, as shown in Figure 3. We have

$$\lambda\varphi_i + \lambda(\hat{n}_i + 1) = \|\hat{\ell} - \rho_i\|_2 + \delta_i$$

for some small positive φ_i . There might not be any cell with label

$$\{\hat{n}_1, \dots, \hat{n}_{i-1}, \hat{n}_i + 1, \hat{n}_{i+1}, \dots, \hat{n}_m\} ,$$

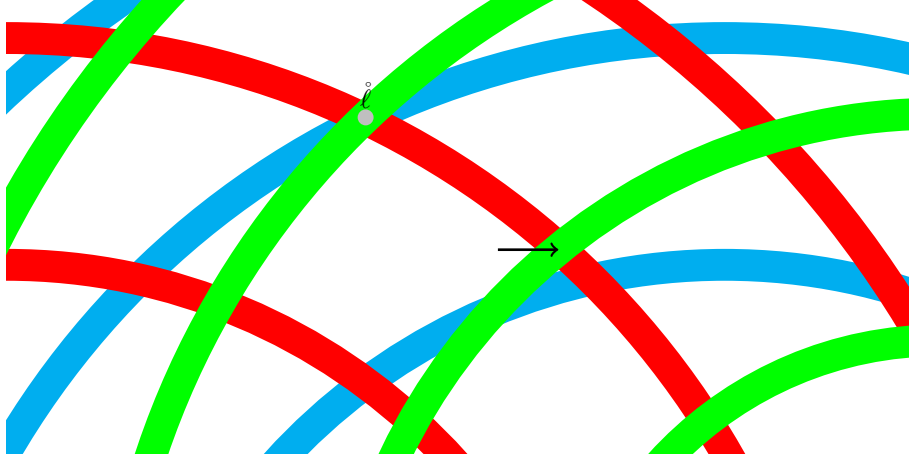


Figure 4: An illustration of 3 families of annuli, depicted in red, green, and cyan. The arrangement has only one cell that is an intersection of one annulus from each family, and in this case it indeed contains the target $\hat{\ell}$, represented by a gray dot. The arrangement also contains one almost-intersection, indicated by the arrow.

as shown in the figure, and the residual

$$\lambda\varphi_i + \lambda\hat{n}_i - \left\| \hat{\ell} - \rho_i \right\|_2$$

will be large, around λ , much larger than $\sigma(\delta_i)$. This shows that this particular construction cannot always handle observation constraints, even when they are guaranteed to be much smaller than λ . Note that when $\|\hat{\ell} - \rho_i\|$ is close to a multiple of λ , this failure can occur with a significant probability. The next constructions that we propose avoid this failure mode.

7.3 Intersections of Families of Annuli

The constraint

$$\lambda\varphi_i + \lambda\hat{n}_i = \left\| \hat{\ell} - \rho_i \right\|_2 + \delta_i$$

together with assumed bounds $|\delta_i| \leq D_i$ constrains $\hat{\ell}$ to a family of concentric annuli (that is, to the union of the annuli in the family)

$$\lambda\varphi_i + \lambda n_i - D_i \leq \|\ell - \rho_i\|_2 \leq \lambda\varphi_i + \lambda n_i + D_i,$$

where $\underline{n}_i \leq n_i \leq \bar{n}_i$. We can derive a bound D_i that holds with high probability from the known distribution of δ_i , say $D_i = 6\sigma(\delta_i)$.

The target $\hat{\ell}$ lies not only in one of the annuli whose center is ρ_i , but also in one annulus in each of the other $m - 1$ families induced by the other $m - 1$ carrier-phase constraints., as shown in Figure 4

Importantly, assuming also that $D_i < \lambda/2$, the annuli in each family are disjoint.

We can exploit these insights by building an arrangement of up the $2mE$ spheres

$$\begin{aligned} \|\ell - \rho_i\|_2 &= \lambda\varphi_i + \lambda n_i + D_i \\ \|\ell - \rho_i\|_2 &= \lambda\varphi_i + \lambda n_i - D_i \end{aligned}$$

for $\underline{n}_i \leq n_i \leq \bar{n}_i$. We then enumerate the cells of the arrangement. For each cell, we determine whether it is part of an annulus of each family, or else lies in the space between two annuli associated with some $n_{i,j}$ and $n_{i,j} + 1$. If the cell is an intersection of m annuli, we find the minimizer $\hat{\ell}(n)$ where n is the label of the cell. When the enumeration ends, we output the minimizer with the smallest residual.

7.4 Near Intersections of Families of Annuli

We now present an effective approximation of the algorithm from Section 7.3 that is useful in the typical case in which $D_i \ll \lambda$.

We start with just two or three families (in 2D or 3D, respectively). Let us consider the 2D case for concreteness, denoting the two selected families by i' and i'' . We compute all the intersections of a circle $\lambda\varphi_{i'} + \lambda n_{i',j'} = \left\| \hat{\ell} - \rho_{i'} \right\|_2$

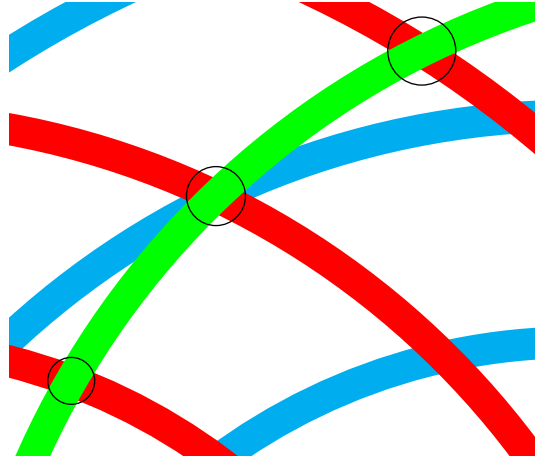


Figure 5: The approximation to an arrangement of annuli. The circle from the green family, centered at ρ_3 , intersects three circles from the red family, centered at ρ_2 . The blue family disqualifies the bottom-left and top-right intersections, because no annulus from the blue family intersects the disks centered at the intersections. Note that the closer the intersection angle to $\pi/2$, the smaller the covering disk.

and a circle $\lambda\varphi_{i''} + \lambda n_{i'',j''} = \left\| \hat{\ell} - \rho_{i''} \right\|_2$, for all admissible integers $n_{i',j'}$ and $n_{i'',j''}$ (intersections of three spheres in 3D). There are $O(E^2)$ such points, $O(E^3)$ in 3D. Each such point p is in the intersection of an annulus from family i' and an annulus from i'' . We now determine whether the intersection of these two annuli contains a cell that is the intersection of one annulus from each of the m families. Our rule to determine this is approximate, but only produces false positives. That is, when our rule indicates that intersection of the two annuli does not intersect all the other annuli, that determination is always correct. When our rule indicates that the intersection also intersects all the other annuli, that might be false in rare cases.

The intersection of two annuli in the plane is not necessarily a shape that resembles a generalized parallelogram, so we begin with an easy-to-check admissibility criterion.

Definition 2. The intersections of two annuli in the plane

$$\begin{aligned} \{\ell \mid r_i - D_i \leq \|\ell - \rho_i\| \leq r_i + D_i\} \\ \{\ell \mid r_{i'} - D_{i'} \leq \|\ell - \rho_{i'}\| \leq r_{i'} + D_{i'}\} \end{aligned}$$

are called *generalized parallelograms* if the two pairs of concentric circles bound them

$$\begin{aligned} \|\ell - \rho_i\| &= r_i \pm D_i \\ \|\ell - \rho_{i'}\| &= r_{i'} \pm D_{i'} \end{aligned}$$

intersect at exactly 8 points.

Figure 6 illustrates two cases in which the intersections of two annuli are admissible and form two generalized parallelograms (top), as well as inadmissible cases in which the four circles intersect at only 6 points (bottom left) or only 4 points (bottom right).

Definition 3. The *center* of a generalized parallelogram defined by the four circles

$$\begin{aligned} \|\ell - \rho_i\| &= r_i \pm D_i \\ \|\ell - \rho_{i'}\| &= r_{i'} \pm D_{i'} \end{aligned}$$

is the point that satisfies the two equations

$$\begin{aligned} \|\ell - \rho_i\| &= r_i \\ \|\ell - \rho_{i'}\| &= r_{i'} . \end{aligned}$$

There are two points that satisfy the two equations, one in each generalized parallelogram. It is easy to see (see 6) that the distance between the center of a generalized parallelogram and ρ_i and $\rho_{i'}$ can be either greater or

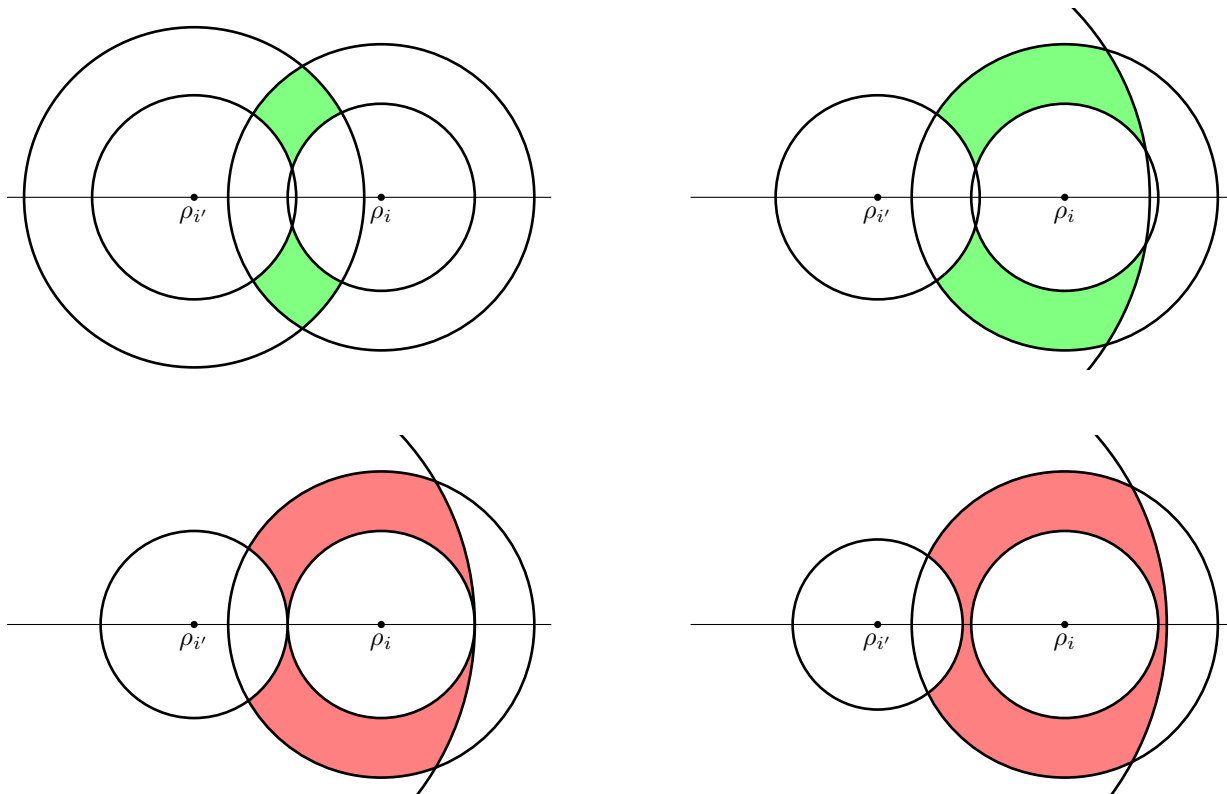


Figure 6: Diagrams that illustrate the definition of generalized parallelograms. Top: the circles that define two annuli intersect at 8 points so the intersection of annuli forms two generalized parallelograms, shown in green. Bottom: the circles intersect at only 6 or 4 points, so the intersections of the two annuli, shown in red, are not considered generalized parallelograms.

smaller than the distance between the center and a corner of the generalized parallelogram. (For the former case, imagine a tiny parallelogram formed by two very thin annuli; for the latter, imagine a long and thin parallelogram that is almost a half circle.)

Our algorithm works as follows. We compute the four or six corners of the generalized parallelogram or parallelepiped and determine the maximum distance $\delta_{i',i''}$ from its center to a corner. We prove below that under very mild conditions, a ball of radius $\delta_{i',i''}$ centered at the center of the generalized parallelogram/parallelepiped covers the parallelogram/parallelepiped, as shown in Figure 5. We now iterate over all the other families, computing the nearest annulus from each family to p . If that annulus does not intersect the ball centered at p , we discard the intersection p because we know that there is no intersection of all m annuli near p . If one annulus from each family intersects the ball, we declare p to be a *near intersection* and we evaluate $\ell(\hat{n})$. This algorithm enumerates all the intersections of m annuli, and perhaps some spurious vectors n that do not correspond to an actual intersection cell. The complexity of generating the candidate integer vectors is $O(mE^2)$ or $O(mE^3)$.

We now prove the claim that the disk or ball cover the generalized parallelogram or parallelepiped. We start with a technical lemma that shows that the central angles defined by sides of generalized parallelograms are smaller than π .

Lemma 4. *The central angles defined by sides of a generalized parallelogram are smaller than π .*

Proof. The 8 intersections of the two pairs of circles are symmetric about the line incident on the two centers (shows as a thin horizontal line in Figure 6). We claim that a generalized parallelogram must be contained in a half plane defined by this line.

The assumption that the 4 bounding circles intersect at 8 points implies that the two open disks $\|\ell - \rho_i\| < r_i + D_i$ and $\|\ell - \rho_{i'}\| < r_{i'} + D_{i'}$ must intersect, which means that the line segment between ρ_i and $\rho_{i'}$ is not in the intersection of annuli.

The same assumption also implies that $r_i + D_i < \|\rho_i - \rho_{i'}\| + r_{i'} - D_{i'}$, otherwise the circle $\|\ell - \rho_i\| = r_i + D_i$ does not intersect the circle $\|\ell - \rho_{i'}\| < r_{i'} - D_{i'}$; similarly $r_{i'} + D_{i'} < \|\rho_i - \rho_{i'}\| + r_i - D_i$ (this case is illustrated in the bottom right diagram in Figure 6). Therefore, the rays that emanate outward from ρ_i and $\rho_{i'}$ along the line connecting them are also not in the intersection of annuli.

Therefore, the entire line connecting the two centers is outside the intersection of the two annuli, which implies that the intersection occupies disjoint areas in the two half planes defined by this line. This proves the claim. \square

We now state and prove a second technical lemma.

Lemma 5. *Let K be a closed disk. Let s and t be points on a circle O with center $\rho \notin K$. Then if $s \in K$ and $t \in K$, then the shorter of the two arcs \overline{st} that form O is also in K .*

Proof. Figure 7 (left) illustrates the notation used in the proof. Suppose for contradiction that there is a point q' on the short arc \overline{st} of O . Since s, t are in K and q' is not, O and the circle C that bounds K must intersect at exactly two points, and these points must be on this shorter arc of O . Therefore, the longer arc of O bounded by s and t , is inside the disk, and so is the chord $s \leftrightarrow t$. The shape bounded by this long arc and the chord is convex. Its boundary is inside K so its interior is also in K . This interior includes the center ρ of O . We conclude that ρ is in K , which contradicts our assumptions. \square

Next, we state and prove the theorem that guarantees that the disk that our algorithm constructs covers the generalized parallelogram in two dimensions. We provide two proofs. One is intuitive but requires a very mild condition. The second is more technical but does not require the additional condition. Note that both proofs state a slightly more general claim, which allows p to be any point in the generalized parallelogram.

Theorem 6. *Let A be a closed generalized parallelogram formed by the intersection of two annuli,*

$$\begin{aligned} r_i - D_i &\leq \|\ell - \rho_i\| \leq r_i + D_i \\ r_{i'} - D_{i'} &\leq \|\ell - \rho_{i'}\| \leq r_{i'} + D_{i'} \end{aligned}$$

for some $0 < D_i, D_{i'}$. Let p be some point in the interior of A and let \bar{p} be the furthest corner of the generalized parallelogram from p . That is, \bar{p} lies on both $\|\ell - \rho_i\| = r_i \pm D_i$ and $\|\ell - \rho_{i'}\| = r_{i'} \pm D_{i'}$ and it maximizes $\|p - \bar{p}\|$.

Let K be the closed disk $K = \{\ell \mid \|\ell - p\| \leq \|\bar{p} - p\|\}$ and let $C = \partial K$ be the circle that is the boundary of K .

The first proof of the theorem also requires that ρ_i and $\rho_{i'}$ are outside K .

The disk K contains the generalized parallelogram A ,

$$A \subseteq K .$$

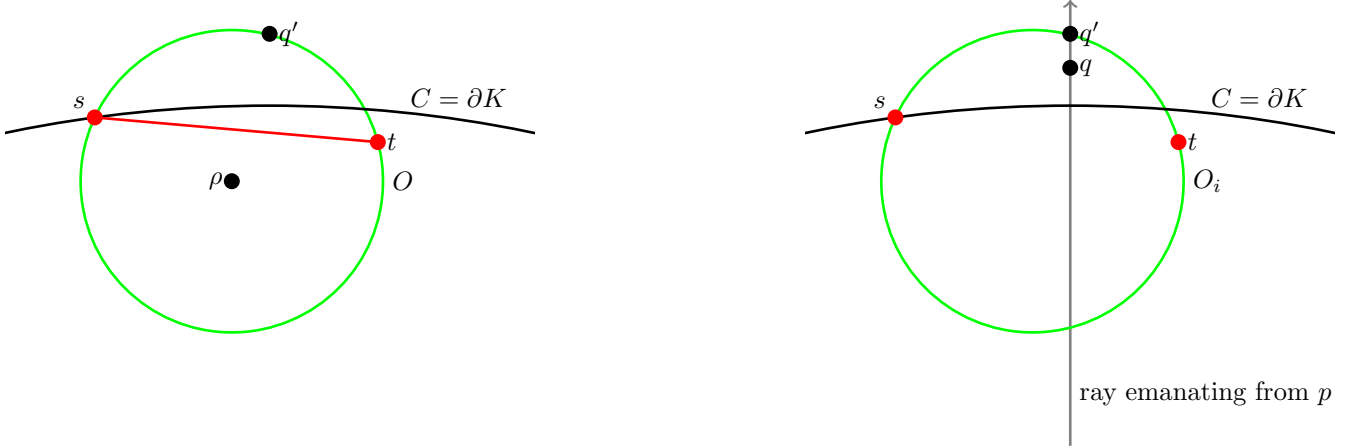


Figure 7: Diagram to illustrate the proofs of Lemma 5 (left) and Theorem 6 (right).

Proof. Figure 7 (right) illustrates the notation that is used in the lemma. Suppose for contradiction that there is a point $q \in A$ that is not in the disk K . We first claim that there must also be a point $q' \in A$, $q' \notin K$ that lies on one of the four circles $\|\ell - \rho_i\| = r_i \pm D_i$, $\|\ell - \rho_{i'}\| = r_{i'} \pm D_{i'}$. If q already lies on one of the four circles, there is nothing to prove. Otherwise, consider the ray emanating from p and passing through q . The ray starts at p (the center of K), which is both in A and in K . When the ray reaches q , it is in A (by definition of q) but outside K . Points even further from q along the ray are all outside K . Since A is bounded, the part of the ray that starts at q must intersect the boundary of A . This intersection point satisfies all the conditions that define q' , so we mark it as q' .

Suppose without loss of generality that q' lies on the circle $O_i = \{\ell \mid \|\ell - \rho_i\| = r_i + D_i\}$ and that the corners of A on O_i are s and t . By Lemma 4, the angle $\angle s\rho_i t$ is smaller than π . Therefore, the point q' lies on the shorter arc of O_i bounded by s and t . By Lemma 5, q' is in K , which contradicts our assumptions. \square

Appendix A presents an alternative proof that does not require the hypothesis that ρ_i and $\rho_{i'}$ are outside K . We now prove the containment result in 3 dimensions. Our proof requires an assumption on the central angles, as well as an assumption that the centers ρ_i , $\rho_{i'}$, and $\rho_{i''}$ and the line segments connecting them are outside the ball that the algorithm constructs.

Theorem 7. *Let A be a closed generalized parallelepiped formed by the intersection of three annuli (spherical shells) in $3D$,*

$$\begin{aligned} r_i - D_i &\leq \|\ell - \rho_i\| \leq r_i + D_i \\ r_{i'} - D_{i'} &\leq \|\ell - \rho_{i'}\| \leq r_{i'} + D_{i'} \\ r_{i''} - D_{i''} &\leq \|\ell - \rho_{i''}\| \leq r_{i''} + D_{i''} \end{aligned}$$

for some $0 < D_i, D_{i'}, D_{i''}$. Let p be a point in the interior of A and let \bar{p} be the furthest corner of the generalized parallelepiped from p . That is, \bar{p} lies on three spheres: $\|\ell - \rho_i\| = r_i \pm D_i$, $\|\ell - \rho_{i'}\| = r_{i'} \pm D_{i'}$, and $\|\ell - \rho_{i''}\| = r_{i''} \pm D_{i''}$ and it maximizes $\|p - \bar{p}\|$.

Let \mathcal{K} be the closed ball $\mathcal{K} = \{\ell \mid \|\ell - p\| \leq \|\bar{p} - p\|\}$ and let $\mathcal{C} = \partial\mathcal{K}$ be the sphere that is the boundary of \mathcal{K} .

Suppose further that ρ_i , $\rho_{i'}$ and $\rho_{i''}$ are outside \mathcal{K} , that the 3 line segments that connect ρ_i , $\rho_{i'}$ and $\rho_{i''}$ are also outside \mathcal{K} , and that for any point ρ on one of these segments and any two points $s, t \in A$, the angle $\angle s\rho t$ is smaller than π .

Then

$$A \subseteq \mathcal{K}.$$

Proof. We prove the lemma in two steps, using reductions to Lemma 6. In the first step, we claim that the edges of the parallelepiped are in \mathcal{K} . These edges are arcs of circles, where the circles are the intersections of two spheres out of three, say $\|\ell - \rho_i\| = r_i + D_i$ and $\|\ell - \rho_{i'}\| = r_{i'} - D_{i'}$.

Let s and t be the corners of the parallelepiped at the ends of a particular edge, say the edge that belongs to the two spheres $\|\ell - \rho_i\| = r_i + D_i$ and $\|\ell - \rho_{i'}\| = r_{i'} - D_{i'}$. Consider the restriction of our problem to the plane f that passes through the circle O defined by the intersection of these two spheres. The center ρ of O lies on the line

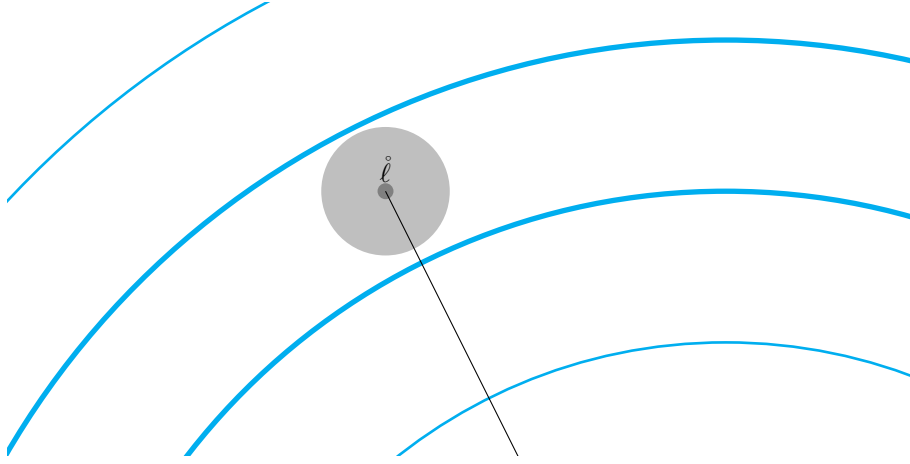


Figure 8: The distance between the target and its inner and outer spheres, depicted using thick lines, bounded from below in Lemma 8. The distance from ρ_i to $\mathring{\ell}$ is $\lambda\mathring{n}_i + \lambda\varphi_i$, to within $\pm \max_i |\delta_i|$, and the radii of the inner and outer spheres are $\lambda\mathring{n}_i - \lambda\varphi_i - \lambda/2$ and $\lambda\mathring{n}_i - \lambda\varphi_i - \lambda/2$.

segment that connects the centers of the two spheres whose intersection defines O , ρ_i and $\rho_{i'}$. This line segment is perpendicular to f . By the hypotheses of the lemma, the line segment is not in \mathcal{K} and therefore $\rho \notin \mathcal{K}$. The restriction of \mathcal{K} to our plane is a disk $K = \mathcal{K} \cap f$. By definition, $s, t \in \mathcal{K} \cap f$, and by our hypotheses, $\angle spt$ is smaller than π . By Lemma 5, the edge that connects s and t is also in $\mathcal{K} \cap f$ and hence in \mathcal{K} . We have established our first claim.

Next, we claim that the faces of the parallelepiped are in K . Let q' be a point on a face of the parallelepiped but not on one of its edges (if it is on an edge, our first claim shows that $q' \in K$). Without loss of generality assume that q' lies on the face that is part of the sphere $\|\ell - \rho_i\| = r_i + D_i$. We now consider the plane f' that passes through ρ_i , q' , and p . The restriction $K \cap f'$ is again a circle whose center is $p \in K \cap f'$. The intersection of sphere $\|\ell - \rho_i\| = r_i + D_i$ that contains the face with f' is also a circle whose center is $\rho_i \in K \cap f'$. The intersection of the face with f' is an arc of this circle. The endpoints s and t of this arc are points that are part of edges of the parallelepiped, which by the first claim is in K . The angle $\angle s\rho_i t$ is smaller than π , so Lemma 5 guarantees that the arc is in K and that, therefore, q' is in K .

Finally, we claim that any point q in the interior of the parallelepiped must also be in K . Let L be an arbitrary line through q , and let S denote the maximal line segment of $L \cap A$ that contains q . By the arguments so far the endpoints of S are in K , hence, by convexity of K , q is in K as well. \square

7.5 Arrangements of Spheres with Shifted Integer Radii

Another way to construct an arrangement with a cell labeled with the correct integer vector is using the families of spheres

$$\lambda n_i + \lambda\varphi_i + \frac{\lambda}{2} = \|\ell - \rho_i\|_2$$

for $\underline{n}_i - 1 \leq n_i \leq \bar{n}_i + 1$. We refer to the circle (or sphere)

$$\lambda n_i + \lambda\varphi_i + \frac{\lambda}{2} = \|\ell - \rho_i\|_2$$

as the i th *outer* circle (sphere) and to

$$\lambda n_i + \lambda\varphi_i - \frac{\lambda}{2} = \lambda(n_i - 1) + \lambda\varphi_i + \frac{\lambda}{2} = \|\ell - \rho_i\|_2$$

as the i th *inner* circle or sphere.

Lemma 8. *Let $D \geq \max_i |\delta_i|$ and assume that $D < \lambda/2$, and let the target $\mathring{\ell}$ lie in the cell labeled \mathring{n} . Then the distance between $\mathring{\ell}$ and the boundary of its cell is at least $\lambda/2 - D > 0$.*

Proof. The radius of the i th inner sphere is $\lambda\hat{n}_i + \lambda\varphi_i - \lambda/2$ and that of the outer sphere is $\lambda\hat{n}_i + \lambda\varphi_i + \lambda/2$. The range to the target satisfies the equation

$$\|\hat{\ell} - \rho_i\|_2 = \lambda\hat{n}_i + \lambda\varphi_i - \delta_i.$$

Therefore, the ranges satisfy the inequalities

$$\begin{aligned} \|\hat{\ell} - \rho_i\|_2 - \left(\frac{\lambda}{2} - D\right) &= \lambda\hat{n}_i + \lambda\varphi_i - \delta_i - \left(\frac{\lambda}{2} - D\right) \\ &\geq \lambda\hat{n}_i + \lambda\varphi_i - \frac{\lambda}{2} \end{aligned}$$

and

$$\begin{aligned} \|\hat{\ell} - \rho_i\|_2 + \left(\frac{\lambda}{2} - D\right) &= \lambda\hat{n}_i + \lambda\varphi_i - \delta_i + \left(\frac{\lambda}{2} - D\right) \\ &\leq \lambda\hat{n}_i + \lambda\varphi_i + \frac{\lambda}{2}. \end{aligned}$$

Therefore, an open ball of radius $\lambda/2 - D$ centered at $\hat{\ell}$ is contained in the annulus that the i th inner and outer spheres define. This implies that the ball is contained in the cell labeled \hat{n} . \square

Once we construct this arrangement, we can enumerate its cells, provably including the one labeled \hat{n} , and minimize $\hat{\ell}(n)$ in each cell. (Correctness depends, of course, on the validity of $|\delta_i| < \lambda/2$, which implies that there is a $D < \lambda/2$ such that $D \geq \max_i |\delta_i|$; note that the construction does not depend on D .)

7.6 Comparison of the Algorithms

We presented in this section three algorithms that can enumerate, with high probability with respect to the distribution of observation errors, a set of integer vectors that contains \hat{n} . Each has advantages and disadvantages:

- The *intersection of annuli* algorithm constructs the largest arrangement, consisting of up to $2mE$ circles or spheres, so it will need to enumerate the largest number of integer vectors (cells in the arrangement). However, most of these cells are not intersections of m annuli, so the continuous nonlinear least-squares minimization to determine $\hat{\ell}(n)$ needs to be carried out just a few times. The theoretical complexity of this algorithm is $O((mE)^2)$ in 2D and $O((mE)^3)$ in 3D; it can be implemented fairly easily in 2D, but not currently in 3D (since there is no existing implementation of the algorithm that constructs an arrangement of spheres).
- The *intersection of circles or spheres* algorithm approximates the previous one. It is easy to implement in both 2D and 3D, its theoretical complexity is lower, $O(mE^2)$ or $O(mE^3)$, but it might run the continuous least-squares minimization on some cells that are not actually intersections of m annuli.
- The *arrangement of circles with shifted integer radii* algorithm constructs a smaller arrangement of at most mE circles. Its theoretical asymptotic complexity is the same as that of the *intersection-of-annuli* algorithm, $O((mE)^2)$ or $O((mE)^3)$, but the smaller arrangement reduces the time and space required to construct it. It can be implemented in 2D but not in 3D. It runs the nonlinear least-squares minimization on all the cells that it enumerates; it has no way to disqualify most of them like the first two methods.

8 Simulations and Evaluation

We conducted extensive analyses of the algorithms on simulated data. The simulations used the parameters shown in Section 2.1 unless noted otherwise. We conducted simulations in both 2D and 3D. Simulation data was generated in Python.

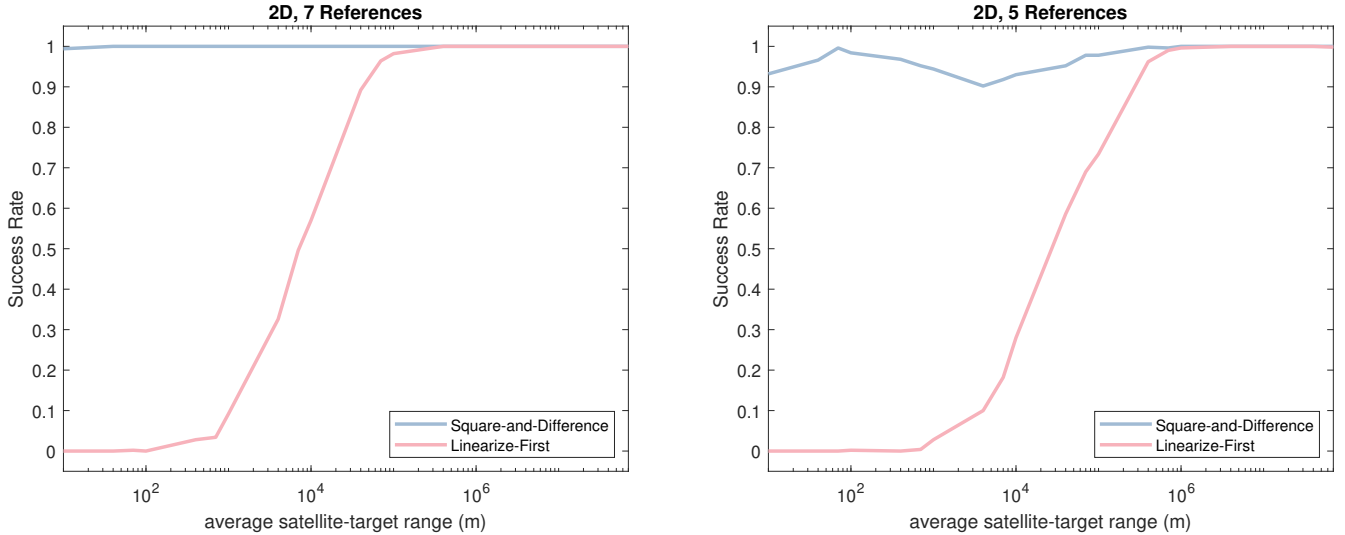


Figure 9: Success rates our new square-and-difference algorithm in two dimensions, compared to that of the linearize-first (LAMBDA) approach. The graphs plot the success rates for problems with 7 and 5 references (left and right).

8.1 Performance of Mixed-Discrete Least-Squares Minimization Algorithms

We implemented the mixed-discrete least-squares minimization algorithms described in Sections 4, 5 and 6 in Python and MATLAB. The parts in MATLAB are mostly the integer or discrete least-squares search algorithms. We use a software package called MILES (Chang and Zhou 2007), implemented in MATLAB, to solve mixed-integer least-squares minimization problems. In other words, the implementations of the LLL algorithm and the Schnorr-Euchner search are the ones in MILES. We note that in early experiments, MATLAB implementations of these algorithms turned out to be much faster in MATLAB than in Python, probably due to the fact that MATLAB uses a just-in-time-compiler.

Figure 9 compares the success rates of our new square-and-difference algorithm relative to those of the linearize-first approach (i.e., LAMBDA) on problems in two dimensions with single-epoch data (one observation of each reference). We define here success as the correct recovery of all the integers, which leads to very accurate localizations.

The data shows that with 7 references, the square-and-difference algorithms returns correct results down to very short ranges, 40 m. Even at 10 m the algorithm succeeds more than 99% of the time. The linearization-first approach, on the other hand, starts to fail with 7 references at ranges of about 40 km, and fails badly at 10 km and below. With only 5 references, the square-and-difference algorithm succeeds about 90% of the time or more, but its performance is certainly worse than with 7 references. The results with 6 references are in between. The performance of the linearization-first approach is also worse than with 7 references; it fails at even longer ranges. We stress that failures in the linearization-first approach are caused by the linearization; the linear mixed-integer least-squares solver returns the optimal solution, but the optimal solution of the linearized problem differs from that of the original nonlinear problem.

The results in three dimensions are qualitatively similar, but more references are required. Our algorithm gets quite slow in 3D at large ranges, so we present its performance at ranges of up to 10 km. Figure 10 shows that with 8 references, our algorithm almost always succeeds in 3D at short ranges, whereas MILES fails completely at the same ranges. With only 7 references, our algorithm succeeds 90% of the time or more, but its performance is clearly worse than with 8 references.

When there are too few constraints, both algorithms fail, as shown in Figure 11. The graphs in the figure show that with 6 references both algorithms achieve a success rate of about 80-90% at either short ranges (our algorithm) or long ranges (LAMBDA) but both fail quite badly at other ranges. With only 5 references, both algorithms fail miserably.

The two algorithms also behave very differently in terms of their computational efficiency, which determines the running times. Figure 12 presents the running times of the algorithms on 2D problems with 8 references at target-reference ranges of 100 m and 100 km. Running times were measured on a computer with an Intel i7-7500U processor running at 2.7 GHz running Windows and MATLAB version 2024a. At short ranges, the running times of the square-and-difference and the linearize-first algorithms are quite similar, with a median running times around

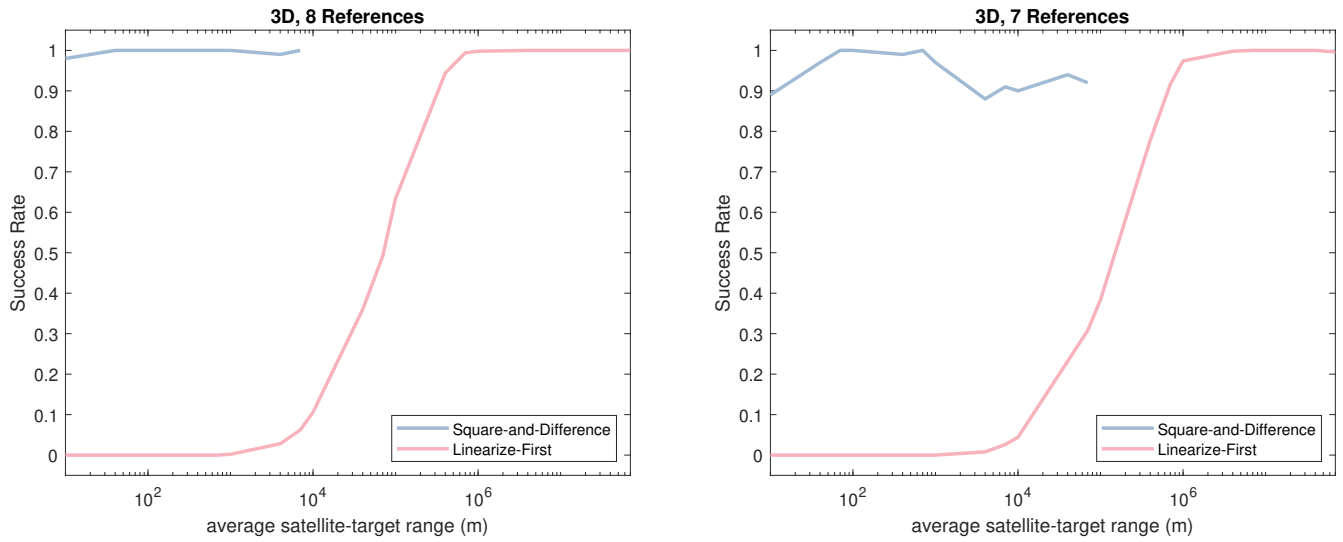


Figure 10: Success rates our new square-and-difference algorithm in three dimensions, compared to that of the linearize-first approach. The graphs plot the success rates for problems with 8 and 7 references (left and right).

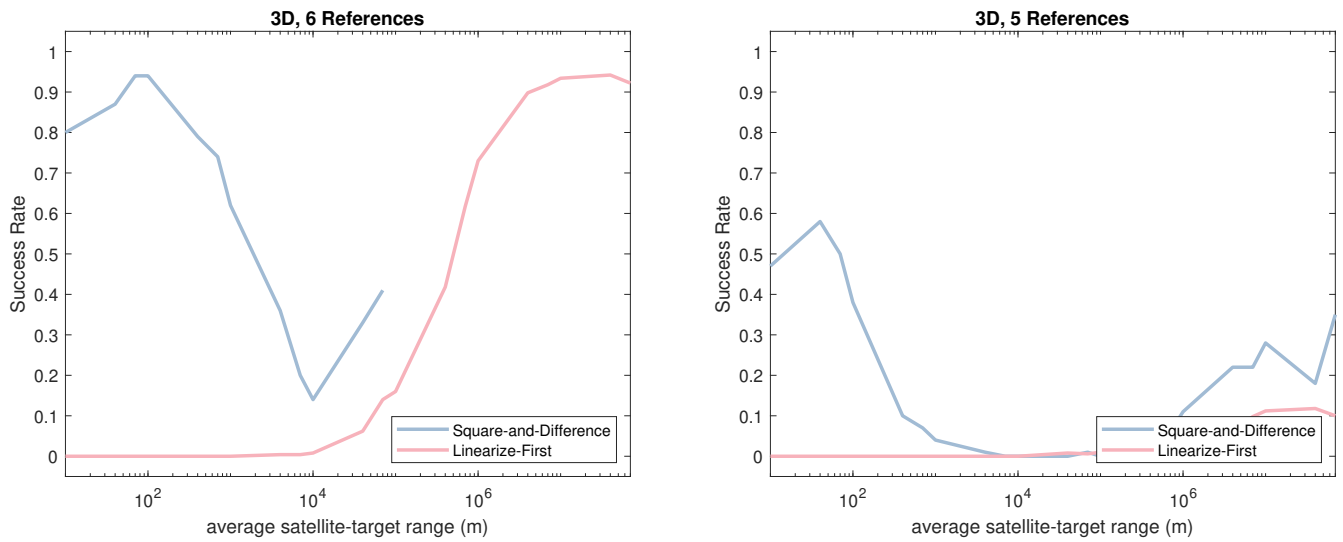


Figure 11: Success rates with too few references.

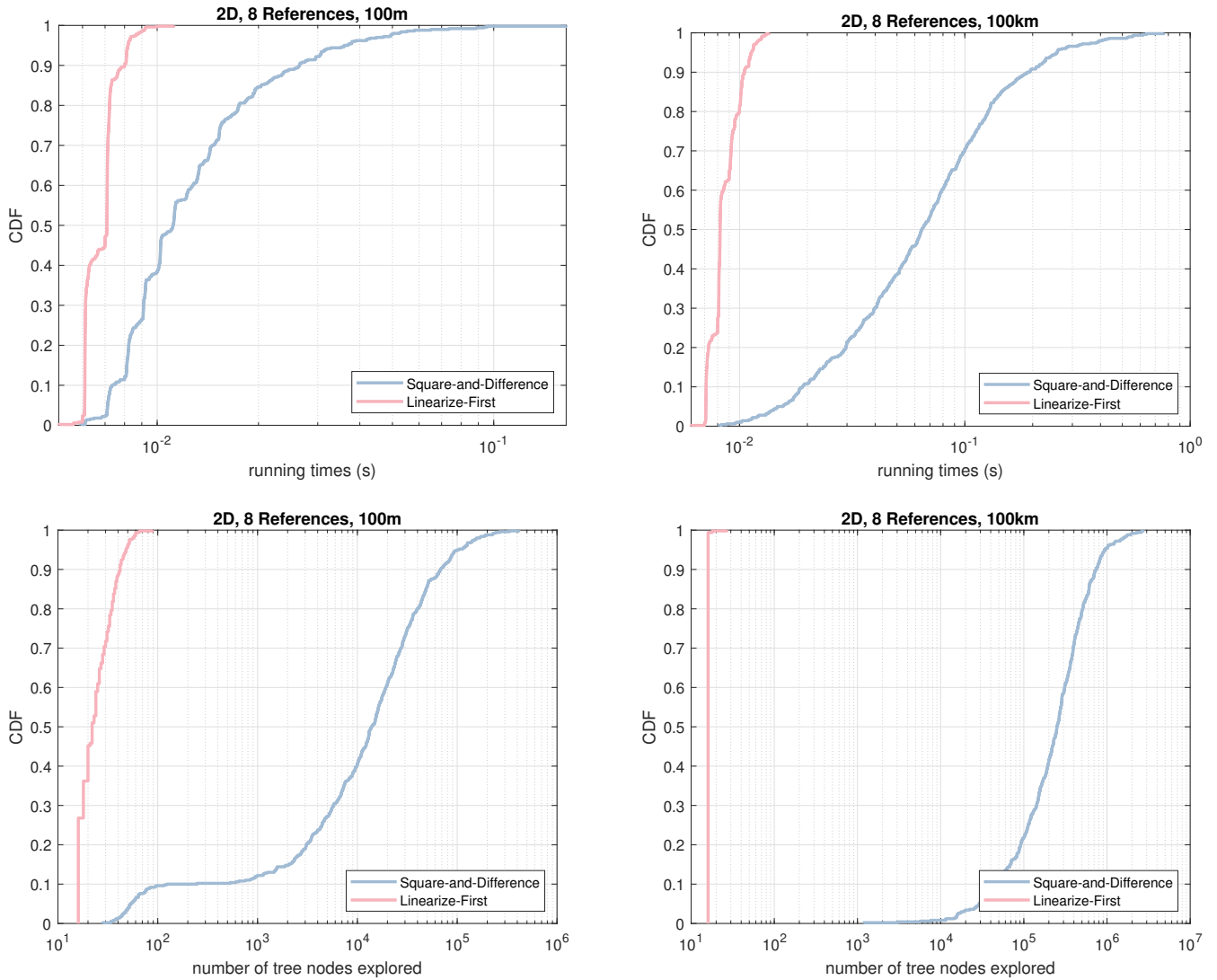


Figure 12: The running times (top row) of the algorithms and the number of tree nodes they explore (bottom row) in two dimensions with 8 references, on ranges of 100 m or 100 km between the target and the references.

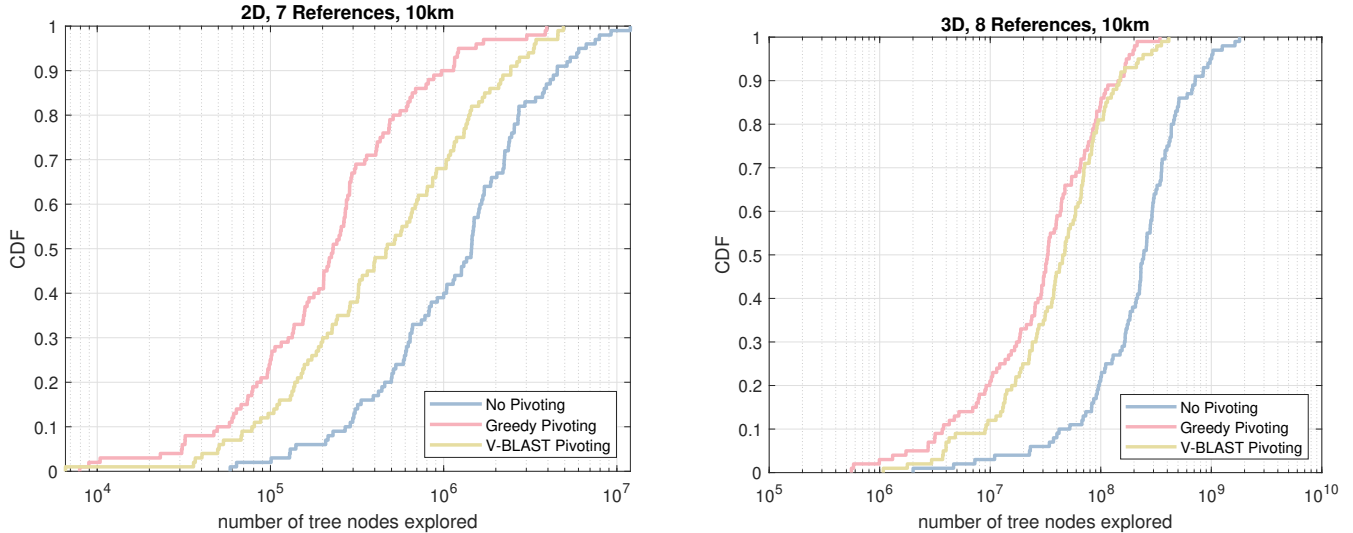


Figure 13: The number of nodes that the square-and-difference algorithm explores during the Schnorr-Euchner search with three different column-ordering strategy: no pivoting, greedy column pivoting, and V-BLAST.

10 ms. Virtually all the runs completed within 100 ms. At ranges of 100 km, in which the linearize-first approach is effective, its running times are short and stable, taking less than 10 ms. The square-and-difference approach is much slower at these large ranges, with a median of over 60 ms and with 10% of the runs taking longer than 200 ms.

The degradation of the performance of the square-and-difference algorithm at high ranges is caused by the $2\delta_i \left\| \hat{\ell} - \rho_i \right\|_2$ term in Equation 7. The algorithm drops this term and compensates with an appropriately-large variance, which forces the search algorithm to consider many more discrete solutions.

The graphs in the bottom row of Figure 12 present the number of tree nodes that the two algorithms explore in the discrete least-squares search. The number of tree nodes is the number of assignments to discrete variables during the Schorr-Euchner search (original or generalized version). The data reveals that at short ranges (100 m), the median number of nodes explored is only 40 in the linearize-first approach, versus more than 6,800 in the square-and-difference approach. The wall-clock running times are similar at this range due to the cost of the LLL basis-reduction step, which is used in the linearize-first approach, which searches over the integers, but not in the square-and-difference approach, which searches over squares of shifted integers.

At ranges of 100 km the linearize-first-approach searches even fewer assignments, almost always 16, but the square-and-difference approach performs even more assignments, median of more than 143,000. This causes this algorithm an appreciable slowdown relative to shorter ranges.¶

Figure 13 shows the effect of different column ordering strategies, discussed in Section 6.2, on the number of nodes explored during the Schnorr-Euchner search. The figure presents results for ranges of 10 km in both 2D and 3D; the results are qualitatively similar for other ranges and numbers of references. We see that the greedy column pivoting strategy, which selects columns from first to last by minimizing the Euclidean norm among remaining columns, reduces the number of nodes searched by about a factor of 10. The more sophisticated V-BLAST strategy, which selects columns from last to first by maximizing diagonal values from last to first, actually performs a little worse than greedy pivoting.

Figure 14 presents the success rates of the multi-epoch square-and-difference algorithm in 2D using 7 references that move in circular orbits, simulating satellites. The graph on the left shows that when the references move at high speed, 200 m/s, our algorithm solves for the correct integers almost 100% of the time, even at short ranges. The linearize first approach works well at large ranges but fails at short one, just like with one epoch. When the references move more slowly, at 30 m/s, the estimation problem becomes harder and our algorithm recovers the integers correctly only about 85% of the time at short ranges.

Figure 15 shows that the behavior of the algorithms in 3D is similar. With 10 high-velocity references, moving at 1000 m/s, our algorithm succeeds nearly 100% of the time down to about 40 m. When the references move at only 30 m/s, performance degrades; our algorithm recovers the integers correctly only 60–90% of the time at distances smaller than about 10 km.

Note that the failures of the squaring and double-differencing method at slow reference velocities can be avoided by running the single-epoch method on each epoch separately. As shown in Figure 10, this approach works correctly

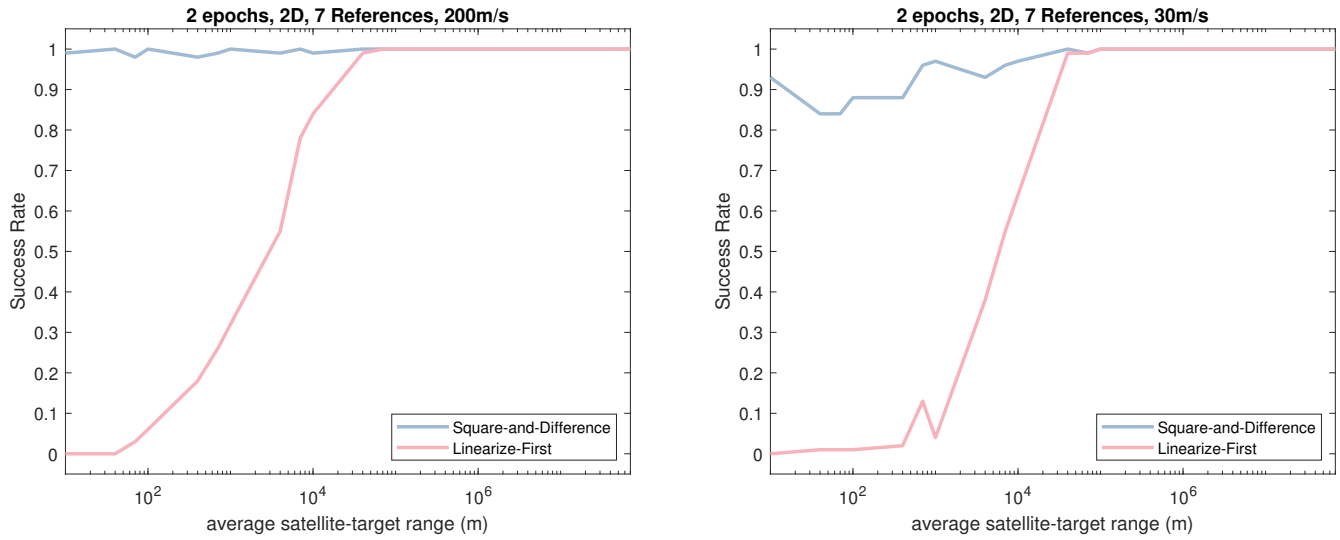


Figure 14: Success rates our new square-and-difference algorithm in two dimensions, compared to that of the linearize-first approach. The graphs plot the success rates for problems 7 references moving at velocities of 200 m/s or 30 m/s (left and right).

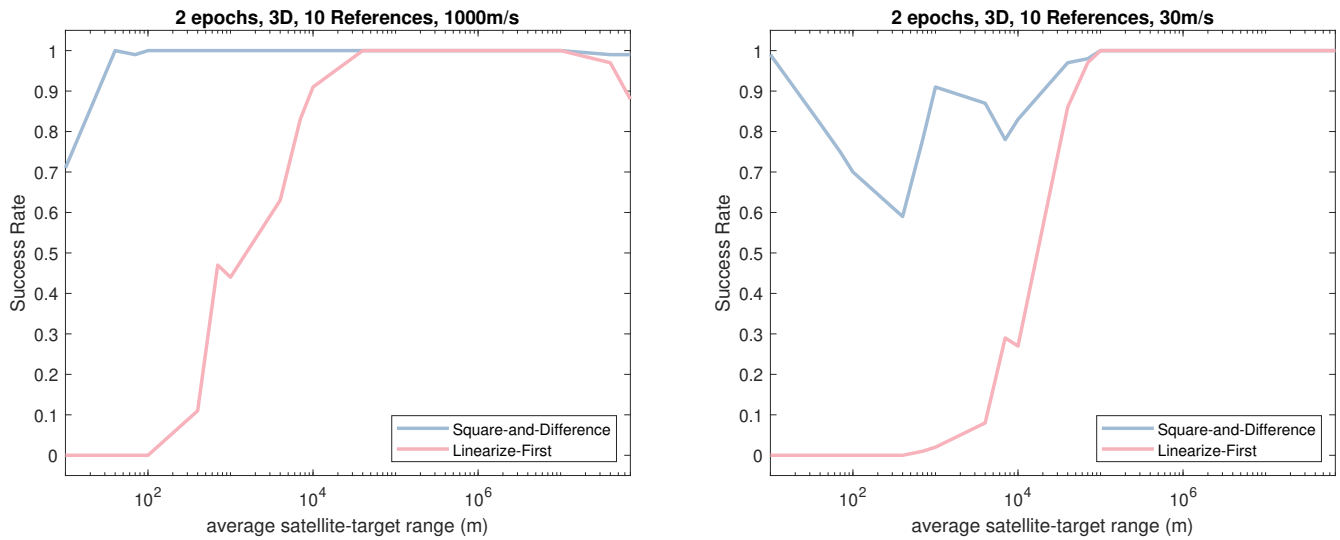


Figure 15: Success rates our new square-and-difference algorithm in three dimensions, compared to that of the linearize-first approach. The graphs plot the success rates for problems with 10 references moving at velocities of 1000 m/s or 30 m/s (left and right).

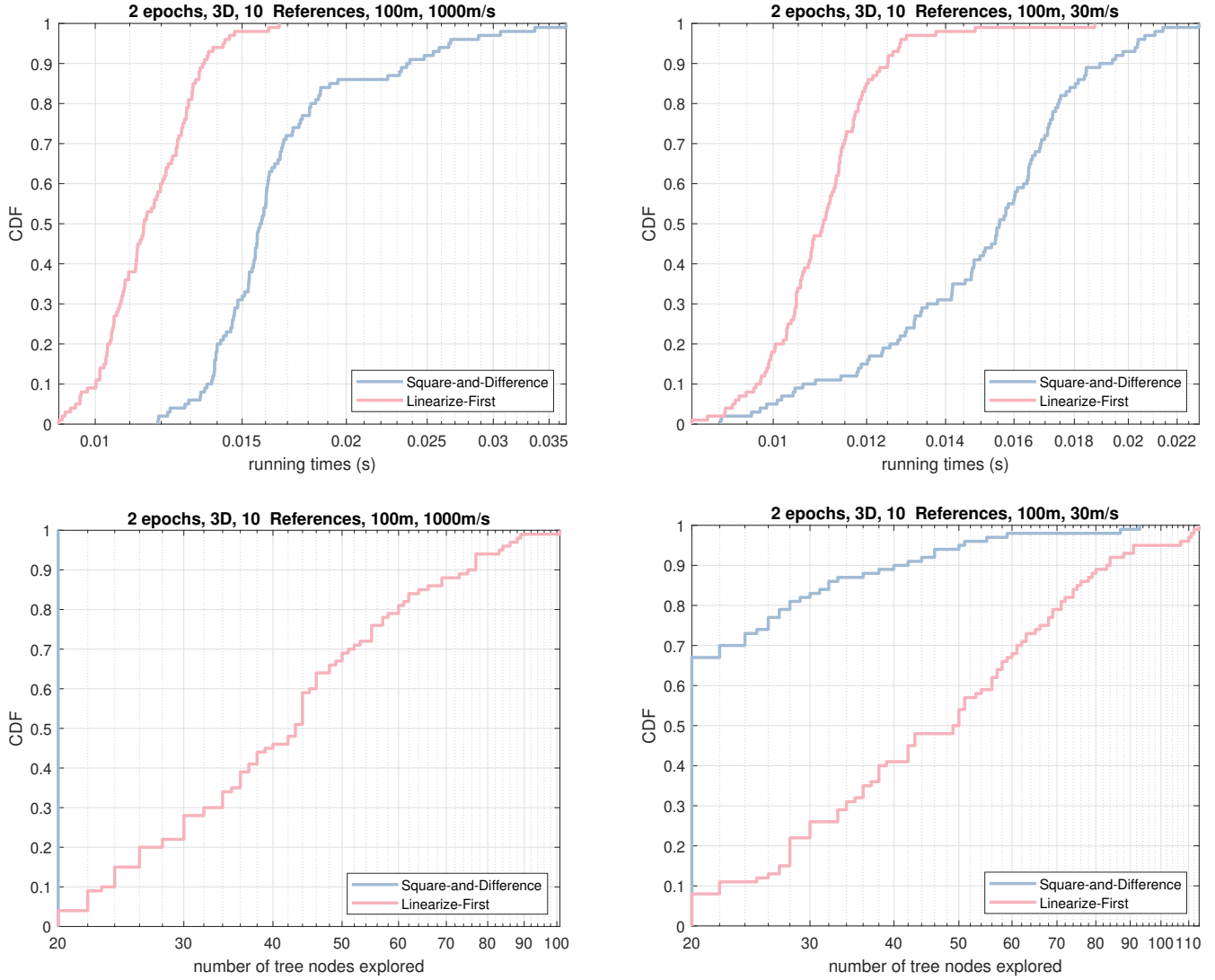


Figure 16: The running times (top row) of the algorithms and the number of tree nodes they explore (bottom row) in 3D and two epochs, with 10 references at a range of 100 m moving at velocities of 1000 or 30 m/s.

even with 8 references. However, the single-epoch method is slower; it does not benefit from the LLL phase so it explores many more assignments of the discrete parameters.

Figure 16 presents the running times and the number of nodes explored in the two-epoch 3D case, using 10 references moving at 1000 or 30 m/s. With fast-moving references, the median running time of our algorithm is 16 ms. Most of the time is spent in the LLL phase; the number of nodes explored is small, with a median of 44. The linearize-first algorithm is a little faster, but not by much: its median running time is over 11 ms. The performance, in terms of running times and number of nodes explored, are not influenced significantly by the velocity of references; the medians at 30 m/s are similar.

8.2 Performance of Geometric Approaches

We implemented the three geometric approaches described in Section 7:

- The method that enumerates intersections and near-intersections of annuli (spherical rings in 3D), described in Section 7.4. We implemented this method in Python using 64-bit floating-point arithmetic. In this method, we choose two or three references arbitrarily (in 2D and 3D, respectively), compute all the intersections of one circle or sphere centered at each reference, and checking that a circle or sphere centered at each other reference ρ_i passes within distance D_i of the intersection. The radii of the circles/spheres is shifted by $\lambda\varphi_i$ from an integer multiple of the wavelength λ . We normally set $D_i = 100\sigma(\delta_i) \approx 5$ mm. This implementation

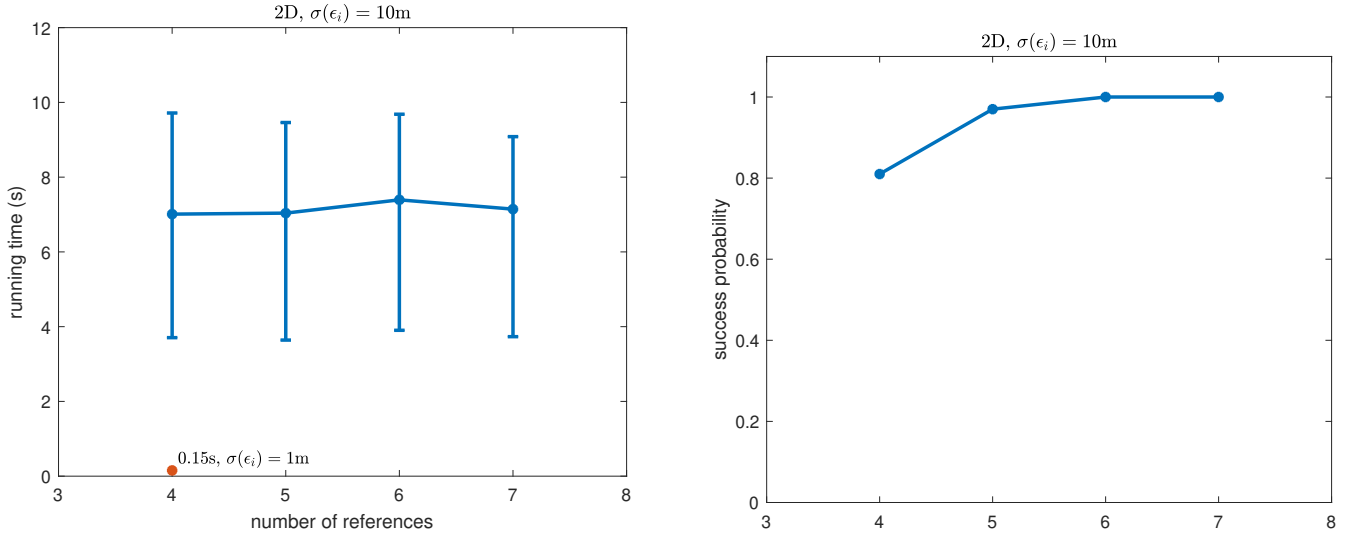


Figure 17: Running times and success rates of the intersection-of-circles as a function of the number of references (left and right). The reported running times (circular dots) are medians and the error bars indicate the 5% and 95% percentiles. The red dot near the bottom of the graph on the left shows the median running time when $\sigma(\epsilon_i)$ is only 1 m, not 10 m.

is much faster than the others, both because of its lower asymptotic complexity and because of the use of floating-point arithmetic. We refer to it as the *intersection of circles*.

- The intersection-of-annuli method, described in Section 7.3. This method is implemented using the CGAL C++ computational-geometry library (The CGAL Project 2024), with a Python interface. CGAL uses a combination of floating-point arithmetic and symbolic computation to ensure that floating-point errors do not cause its algorithms to fail. This method is only implemented in 2D because CGAL currently supports arrangements of circles but not arrangements of spheres. We set the width of the annuli to $1000\sigma(\delta_i) \approx 50$ mm. We refer to this implementation as the *intersection of annuli*.
- A simplified version of the method that computes the geometric arrangement of circles with shifted integer radii, described in Section 7.5. Our implementation shifts the circles by $\lambda\varphi_i$, not by $(\lambda/2)\varphi_i$. The algorithm constructs the arrangement and then enumerates its vertices, checking the residual norm in each of them. Normally, one or a few have very low residual norms, including one near the target. The cost of constructing this arrangement is essentially the same as that of the method proposed in Section 7.5, with the $(\lambda/2)\varphi_i$ shift. This method also uses CGAL through a Python interface, and it is only implemented in 2D, due to the same limitation of CGAL. We refer to this method as the *arrangement of circles* method.

All the implementations enumerate a set of vertices or cells, and when they enumerate cells, they also identify a point in the cell. Each vertex or cell maps to a set of integers. The implementations then solve the continuous nonlinear least squares (with the integers resolved) starting at the vertex or point in the cell to find the least-squares optimal solutions.

All the implementations filter out candidates that are more than $3\sigma(\epsilon_i)$ from the minimizer of the range constraints (equivalent to the code-phase solution in GNSS). This is a little aggressive and is likely to cause failures in about 1% of the tests. Using a more conservative bound, say $6\sigma(\epsilon_i)$, would reduce the failure rate but would increase the running time because this would generate a factor of 4 or 8 (in 2D or 3D) more candidate locations.

All the test problems use a mean reference range of just 100 m, carrier-phase errors with standard deviation $\sigma(\delta_i) = 0.1^\circ = 19/3600$ cm, as specified in Section 2.1, and range-measurement errors with standard deviation $\sigma(\epsilon_i) = 10$ m, as specified in Section 2.1, or a tighter $\sigma(\epsilon_i) = 1$ m. The smaller range-measurement errors lead to fewer candidates locations, speeds up the algorithm, and allows us to explore more scenarios.

Each scenario was repeated 100 times using random data.

Figure 17 shows the performance of the intersection-of-circles algorithm. On our standard test setup, with $\sigma(\epsilon_i) = 10$ m, the code takes about 4-10 s to run, essentially independently of the number of references. With 6 or 7 references, the algorithm always filters all the intersections but one, correctly resolving all the N_i s. With 4 and 5 references the algorithm sometimes identifies more than one admissible intersection, leading to correction resolution

of the N_i s in 81% and 97% of the cases, respectively. The number of intersections within $3\sigma(\epsilon_i)$ from the minimizer of the range constraints ranges from about 2.4 k to about 93 k. The running times are highly correlated with the number of intersections.

Reducing $\sigma(\epsilon_i)$ to 1 m reduces the running time by about a factor of 50, from a median of 7 s to a median of 1.5 s. The reduction results from a factor-of-100 shrinkage in the area within the radius- $3\sigma(\epsilon_i)$ disk.

Figure 18 describes the results of experiments in 2 dimensions with all three methods, with both 4 and 8 references. We performed these experiments with $\sigma(\epsilon_i) = 1$ m in order to achieve more reasonable running. The running times of the intersection-of-circles are much faster than those of the methods that rely on constructing arrangements. The running times of the intersection-of-circle are also insensitive to the number of references, as we have seen already in Figure 17, whereas the running times of the arrangement-constructing methods depend strongly on the number of references. This is expected, since their theoretical complexity scales quadratically with the number of references. These scaling behaviors are also evident in the graphs that describe the number of vertices, cells, or intersections that the methods inspect.

We also see, in the bottom row, that the number of admissible cells shrink dramatically as the number of references increases. This phenomenon makes more likely that the integers are resolved correctly.

We also verified that the intersection-of-circles method works correctly in 3D, where each intersection is defined by three spheres. We only ran the method on 5 random test cases, due to the long running times. We used 7 references, $\sigma(\epsilon_i) = 10$ m, and set $D_i = 1000\sigma(\delta_i) \approx 50$ mm. The algorithm correctly resolved the integers in all cases. The median running time was a little over an hour (range of 3274–3810 s) and the median number of intersections was about 5 M (range of 4.3–19.0 M).

9 Conclusions

The use of simplified system model, in which the system observes the range of a target from a number of references both directly and in the carrier-sense (remainder) sense, allowed us to demonstrate that LAMBDA approaches are inappropriate for carrier-phase localization at short ranges, and allowed us to develop a range of algorithms that are effective at short ranges.

The failure of LAMBDA at short ranges stems from the large linearization error. There is no doubt that the same failure also occurs in more realistic system models with nuisance parameters, like the models that are routinely used for carrier-phase localization in GNSS.

Our results also outline very clearly the research that still needs to be conducted before we have effective algorithms for carrier-phase localization at short ranges. We need to investigate which of the methods that we proposed in this paper can be extended to more realistic system models, and how.

Another challenge is performance, in the sense of running time and parallelization. Our implementations, especially of the square-and-difference algorithms, perform well in many cases, but in general they are more expensive than the LAMBDA approach. However, even the fastest geometric algorithm (intersections of circles) is much slower than the square-and-difference algorithms. Additional work is required to develop more efficient variants of our new algorithms, to optimize their implementations, and to create implementations that can exploit multiple cores and/or accelerators like GPUs.

Acknowledgments We thank Xiao-Wen Chang for several insightful discussions and for helpful comments on early versions of the manuscript and for providing us an implementation of his V-BLAST algorithm. We thank Hector Rotstein for many comments and suggestions that improved the article. This research was supported in part by grants from the Blavatnik Computer Science Research Fund. Work by D.H. and E.F. has also been supported in part by the Israel Science Foundation (grant 3598/25).

Competing Interests The authors declare none.

References

- Agrell, E. et al. (2002). “Closest point search in lattices”. In: *IEEE Transactions on Information Theory* 48, pp. 2201–2214. DOI: 10.1109/TIT.2002.800499.
- Bancroft, Stephen (1985). “An algebraic solution of the GPS equations”. In: *IEEE Transactions on Aerospace and Electronic Systems* AES-21.7, pp. 56–59. DOI: 10.1109/TAES.1985.310538.

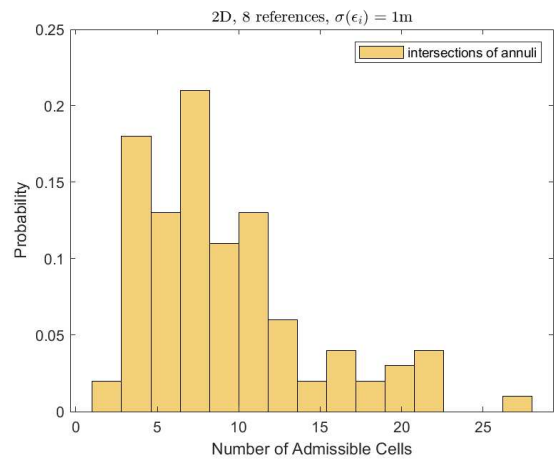
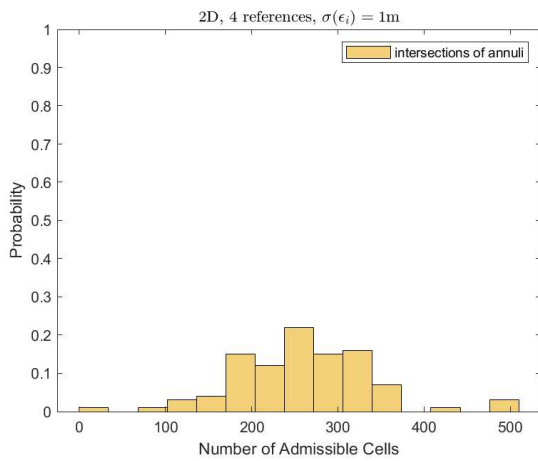
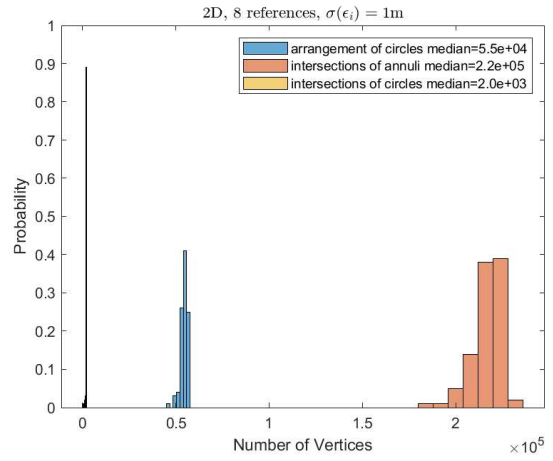
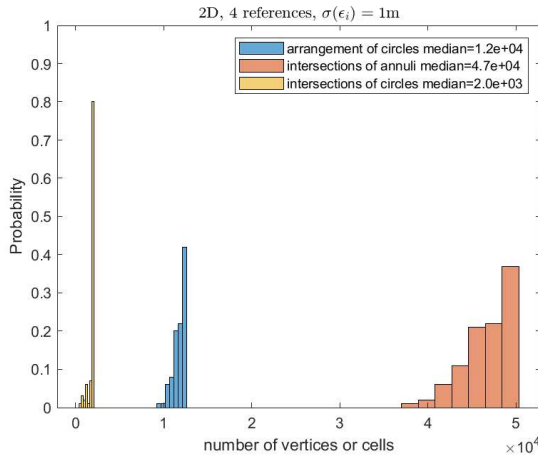
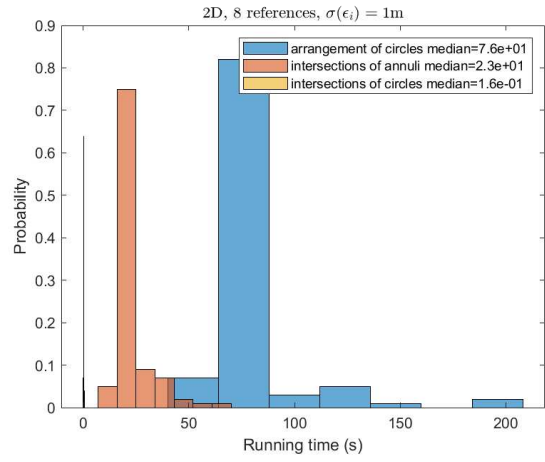
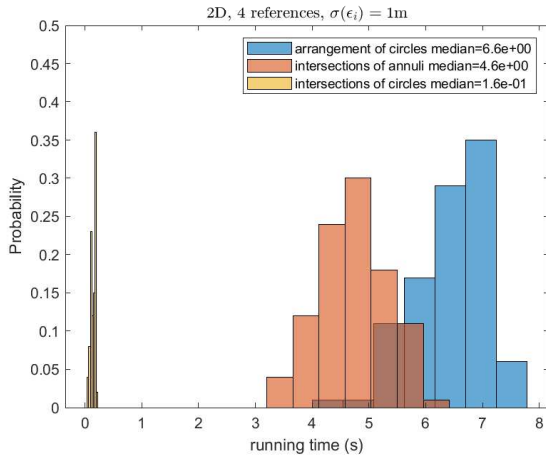


Figure 18: The running times (top row) and number of candidates tested (middle) in all three implementations, as well as the number of intersection cells (bottom) in the intersection-of-annuli implementation.

- Bernstein, Dennis S. (2005). *Matrix Mathematics: Theory, Facts, and Formulas*. Princeton, NJ: Princeton University Press. ISBN: 978-0-691-11393-8.
- Borno, M. A., X.-W. Chang, and X. H. Xie (2014). “On decorrelation in solving integer least squares problems for ambiguity determination”. In: *Survey Review* 46, pp. 37–49. DOI: 10.1179/1752270612Y.0000000029.
- Chang, X.-W., X. Yang, and T. Zhou (2005). “MLAMBDA: a modified LAMBDA method for integer least-squares estimation”. In: *Journal of Geodesy* 79, pp. 552–565. DOI: 10.1007/s00190-005-0004-x.
- Chang, Xiao-Wen and Christopher C. Paige (2003). “An orthogonal transformation algorithm for GPS positioning”. In: *SIAM Journal on Scientific Computing* 24, pp. 1710–1732.
- (2007). “Euclidean distances and least squares problems for a given set of vectors”. In: *Applied Numerical Mathematics* 57.11, pp. 1240–1244. DOI: 10.1016/j.apnum.2007.01.008.
- Chang, Xiao-Wen and Tianyang Zhou (2007). “MILES: MATLAB package for solving Mixed Integer LEast Squares problems”. In: *GPS Solutions* 11, pp. 289–294. URL: <https://doi.org/10.1007/s10291-007-0063-y>.
- Damen, M. O., H. El Gamal, and G. Caire (2003). “On maximum-likelihood detection and the search for the closest lattice point”. In: *IEEE Transactions on Information Theory* 49.10, pp. 2389–2402. DOI: 10.1109/TIT.2003.817444.
- De Jonge, Paul and Christian Tiberius (1996). *The LAMBDA method for integer ambiguity estimation: implementation aspects*. Tech. rep. LGR-Series number 12. Delft Geodetic Computing Center, Delft University of Technology.
- Dinur, I. et al. (2003). “Approximating CVP to Within Almost-Polynomial Factors is NP-Hard”. In: *Combinatorica* 23.2, pp. 205–243. DOI: 10.1007/s00493-003-0019-y.
- Emde Boas, P. van (1981). *Another NP-complete partition problem and the complexity of computing short vectors in a lattice*. Tech. rep. 81-04. Amsterdam: University of Amsterdam.
- Fan, Shaoshuai et al. (2022). “Carrier Phase-Based Synchronization and High-Accuracy Positioning in 5G New Radio Cellular Networks”. In: *IEEE Transactions on Communications* 70.1, pp. 564–577. DOI: 10.1109/TCOMM.2021.3119072.
- Fogel, Efi, Dan Halperin, and Ron Wein (2012). *CGAL Arrangements and Their Applications—A Step-by-Step Guide*. Vol. 7. Geometry and Computing. Springer. ISBN: 978-3-642-17282-3. DOI: 10.1007/978-3-642-17283-0. URL: <https://doi.org/10.1007/978-3-642-17283-0>.
- Halperin, Dan and Micha Sharir (2017). “Arrangements”. In: *Handbook of Discrete and Computational Geometry*. Chapman and Hall/CRC, pp. 723–762.
- Lenstra, A.K., H.W. Lenstra, and L. Lovász (1982). “Factoring polynomials with rational coefficients”. In: *Mathematische Annalen* 261, pp. 515–534. DOI: 10.1007/BF01457454.
- Luk, Franklin T. and Sanzheng Qiao (2011). “A pivoted LLL algorithm”. In: *Linear Algebra and its Applications* 434.11, pp. 2296–2307. DOI: <https://doi.org/10.1016/j.laa.2010.04.003>.
- Luk, Franklin T. and Daniel M. Tracy (2008). “An improved LLL algorithm”. In: *Linear Algebra and its Applications* 428.11, pp. 441–452. DOI: <https://doi.org/10.1016/j.laa.2007.02.029>.
- Micciancio, D. (2001). “The hardness of the closest vector problem with preprocessing”. In: *IEEE Transactions on Information Theory* 47 (3), pp. 1212–1215. DOI: 10.1109/18.915688.
- Nikonowicz, Jakub et al. (2024). “Indoor Positioning in 5G-Advanced: Challenges and Solution Toward Centimeter-Level Accuracy with Carrier Phase Enhancements”. In: *IEEE Wireless Communications* 31.4, pp. 268–275. DOI: 10.1109/MWC.023.2200633.
- Schnorr, C. P. and M. Euchner (1994). “Lattice basis reduction: Improved practical algorithms and solving subset sum problems”. In: *Mathematical Programming* 66, pp. 181–199. DOI: 10.1007/BF01581144.
- Sirola, Niilo (2010). “Closed-Form Algorithms in Mobile Positioning: Myths and Misconceptions”. In: *Proceedings of the 7th Workshop on Positioning, Navigation, and Communication*. IEEE, pp. 38–44. DOI: 10.1109/WPNC.2010.5653789.
- Teunissen, P. J. G. (1995). “The least-squares ambiguity decorrelation adjustment: a method for fast GPS integer ambiguity estimation”. In: *Journal of Geodesy* 70. DOI: 10.1007/BF00863419.
- Teunissen, Peter J. G. (2017). “Carrier Phase Integer Ambiguity Resolution”. In: *Springer Handbook of Global Navigation Satellite Systems*. Ed. by Peter J. G. Teunissen and Oliver Montenbruck. Springer, pp. 661–720.
- The CGAL Project (2024). *CGAL User and Reference Manual*. 6.0.1. <https://www.cgal.org/>. CGAL Editorial Board.
- Toledo, Sivan (2020). *Location Estimation from the Ground Up*. Philadelphia, PA: SIAM. DOI: 10.1137/1.9781611976298.
- Wymeersch, Henk, Rouhollah Amiri, and Gonzalo Seco-Granados (2023). “Fundamental Performance Bounds for Carrier Phase Positioning in Cellular Networks”. In: *Proceedings of the IEEE Global Communications Conference (GLOBECOM)*, pp. 7478–7483. DOI: 10.1109/GLOBECOM54140.2023.10437902.
- Xie, Xiaohu, Xiao-Wen Chang, and Mazen Al Borno (2012). *Partial LLL Reduction*. arXiv 1204.1398, presented at GLOBECOM 2011. DOI: 10.48550/arXiv.1204.1398.

the ray emanating from o and passing through p . The ray intersects the circle that contains the arc st . We denote the intersection point by p' ; it may lie within the arc st or outside it. We handle the two cases separately.

- If p' lies within the arc, then the line segment between p and p' splits the generalized triangle $\triangle pst$ into two generalized triangles, $\triangle ptp'$ and $\triangle psp'$. Consider a point q in one of them; without loss of generality, we assume that it is $\triangle psp'$. We show below that $q \in K$ by showing $|pq| \leq |ps|$.
- If p' lies outside the arc, assume without loss of generality that t lies in the arc sp' . This implies that the generalized triangle $\triangle psp'$ contains the generalized triangle $\triangle spt$. Consider a point $q \in \triangle spt$, which implies $q \in \triangle psp'$. We show below that $q \in K$ by showing $|pq| \leq |ps|$.

In both cases, the ray from o through q intersects the arc sp' . We denote the intersection point by q' .

We denote distances from p by capital letters:

$$\begin{aligned} Q &= |pq| \\ Q' &= |pq'| \\ P' &= |pp'| \\ S &= |ps| \\ O &= |op| . \end{aligned}$$

Note that $O + P' = |op'| = |oq'| = |os|$. We also denote $D = |oq| - O$, so that $|oq| = O + D$. We claim that $D \leq P'$. This is true since $P' = |pp'| = |op'| - O$ and since $|op'| \geq |oq|$.

We now use the law of cosines to the triangles $\triangle ops$, $\triangle opq$, and $\triangle opq'$. Denoting the angle of $\triangle ops$ at o by θ and the angle of both $\triangle opq$ and $\triangle opq'$ at o by γ , the law of cosines gives:

$$\begin{aligned} S^2 &= O^2 + (O + P')^2 - 2O(O + P') \cos \theta \\ Q^2 &= O^2 + (O + D)^2 - 2O(O + D) \cos \gamma \\ Q'^2 &= O^2 + (O + P')^2 - 2O(O + P') \cos \gamma . \end{aligned}$$

The inequality $\gamma \leq \theta \leq \pi$ implies $\cos \gamma \geq \cos \theta$. We subtract the last equality from the first to obtain

$$\begin{aligned} S^2 - Q'^2 &= -2O(R + P') \cos \theta + 2O(O + P') \cos \gamma \\ &= 2O(R + P') (\cos \gamma - \cos \theta) \\ &\geq 0 , \end{aligned}$$

establishing $Q' \leq S$. We now subtract Q'^2 from Q^2 :

$$\begin{aligned} Q'^2 - Q^2 &= (O + P')^2 - 2O(O + P') \cos \gamma - (O + D)^2 + 2O(O + D) \cos \gamma \\ &= P'^2 - D^2 + 2OP' - 2OD - 2P' \cos \gamma + 2D \cos \gamma \\ &= P'^2 - D^2 + 2O(P' - D) + 2O(D - P') \cos \gamma \\ &= (P'^2 - D^2) + 2O(P' - D)(1 - \cos \gamma) . \end{aligned}$$

The first term is nonnegative since $P' \geq D$, as we have shown above. The second term is also nonnegative because $O > 0$, $P' - D \geq 0$, and $1 - \cos \gamma \geq 0$ (for any γ). We conclude that $Q \leq Q'$. Therefore, $Q \leq Q' \leq S$.

The fact that $Q \leq S$ shows that q is indeed in K , completing the proof of the lemma. □

